C.1.

MEASUREMENT OF LOW FREQUENCY ELECTRIC FIELDS USING ELECTRODELESS BREAKDOWN OF GASES

by

DANIEL E. FRIEDMANN

B.A.Sc., The University of British Columbia, 1979

A THESIS SUBMITTED IN PARTIAL FULFILMENT OF

THE REQUIREMENTS FOR THE DEGREE OF

MASTER OF APPLIED SCIENCE

in

THE FACULTY OF GRADUATE STUDIES

(Engineering Physics)

We accept this Thesis as conforming

to the required standard

THE UNIVERSITY OF BRITISH COLUMBIA

JANUARY 1983

In presenting this thesis in partial fulfilment of the requirements for an advanced degree at the University of British Columbia, I agree that the Library shall make it freely available for reference and study. I further agree that permission for extensive copying of this thesis for scholarly purposes may be granted by the head of my department or by his or her representatives. It is understood that copying or publication of this thesis for financial gain shall not be allowed without my written permission.

Department of ENGINEERING PHYSICS

The University of British Columbia
1956 Main Mall
Vancouver, Canada
V6T 1Y3

Date JAN 18 1983

ABSTRACT

There is a need for an electric field meter to measure environmental fields under high voltage transmission lines and their associated switchyards. This thesis describes a new electric field meter based on the electrodeless breakdown of gases in insulating vessels. When a glass bulb filled with a gas (e.g. neon) is placed in an alternating electric field it emits light in the form of pulses. The number of pulses per cycle of the electric field is proportional to the field magnitude. An electric field meter is constructed by conveying the light from the gas filled glass bulb (the sensor) to an electronic counter (the detector) with an optical fiber. The resulting meter has a low weight, non metallic sensor that can be separated from the detector electronics by any desired distance. The sensor shape dictates its directional sensitivity. A spherical bulb has an isotropic response to the field while a cylindrical bulb gives a maximum response when its axis is aligned with the field direction. The size of the bulb is inversely proportional to the threshold below which the field can not be measured. A 25mm bulb has a 10kv m-1 threshold. The transmission of the light signal from the sensor to the detector is immune to electrical noise. The detector electronics is simple because the field magnitude information is contained in the number of pulses not in the magnitude of the pulses.

This thesis presents the theoretical, experimental and field test results which explain the operation of the meter and substantiates its advantages. The basic physical model for the sensor is established by describing the relation between optical pulses and field magnitude, the effect of sensor shape on this relation, the operation of the sensor in elliptically polarized (including harmonic) fields and the effect of bulb size and gas composition on the phenomena.

The basic practical considerations are investigated by studying the environmental effects on the performance of the meter, the lifetime and stability of the meter, the effect of the sensor on the field being measured and the general engineering of meter.

This work has resulted in a fully tested prototype meter whose basic operation is well understood.

Table of Contents

List of Tables

List of Figures

ACKNOWLEDGEMENT

The initial stimulus for this work came from F. Heminsley who was interested in developing a meter for monitoring environmental fields. The intitial invention resulted from a collaborative effort of Jeff Young and the author which resulted in patent application No. 06/142,815 (US). The author is indebted to R.R. Parsons, R.R. Heering and R.A. Nodwell for the encouragement they provided while the project was being developed in the Applied Science 459 Laboratory. Subsequently during the MASc program the B.C. Science Council not only provided financial support for the project but also encouraged the development to the commercial exploitation of the device. Some financial support for the equipment was also provided by NSERC.

The development of the physical models and the planning and execution of the experiments was a joint effort with F.L. Curzon. Many others have also greatly contributed to the development of experimental facilities, the execution of experiments and the construction of the meter. Most notably M. Feeley, G. Auchinleck, F. Easton, R. Allan, A. Cheuck, E. Williams, L. De Silva, D. Parfeniuk, D. Gayton and P. Wong.

The author is very thankfull to J. Rothe and F. Heminsley for their continuous encouragement and help with field tests.

1.0 INTRODUCTION

Electric power is central to the energy systems of Canada and the developed countries. Even with present efforts to reduce the energy intensiveness of the economy through conservation and higher prices, substantial growth in the electric sector is expected to continue.

To move large amounts of power economically and reliably over long distances, electric utilities need overhead A.C. transmission lines which operate at voltages of 500 kV and above. In 1977 the United States alone had 20,000 km[1] of transmission lines operating at 500 kV. Since then the total length of transmission lines in the U.S. has doubled. Furthermore the voltage of the lines has increased continuously. Lines operating at 765 kV are now common, while experimental lines are being operated at voltages above 1000 kV.

Because of this growth (in mileage and voltage) there is an evergrowing number of people being exposed to increasingly larger electric fields generated by these powerlines and their associated substations. Most of those exposed (especially to the larger fields) work in the electric power industry. However others living and/or operating equipment near powerlines or substations also receive substantial exposure to electric fields.

Accompanying this expansion of the electric power industry there is a growing concern among the public, the Electrical Utilities and the regulatory bodies about the possible health effects of these fields. The concern is exemplified by a number of hearings on the proposed construction of higher voltage lines in the U.S.[2]

There are theoretical reasons to believe that low frequency (50 to 60Hz) electric fields can cause biological effects:

1. neurological or other effects can be caused by 50 - 60Hz body currents induced by the external electric field. Although 60Hz is partially chosen for transmission of AC power because of it being the lowest frequency giving the illusion of continuous lighting with incandescent lamps, it is a hazardous frequency. Experiments[3] show that threshold for stimulation of nerve, skeletal muscle and cardiac muscle are minimal near 60Hz;
2. external fields could directly interfere in biological processes that involve or are affected by the presence of electric fields, such as hormone and enzyme recognition processes on cell membrane surfaces, bone growth processes, etc.;
3. small arc discharges which result when a person at one potential touches an object at another potential may also lead to physiological and psychological effects and
4. unwanted signals is prosthetic devices (fillings in teeth, pacemakers, hearing aids, etc.) can be uncomfortable and dangerous.

These theoretical concerns have been partially supported by experiment. Studies published by Presman[4] of results obtained in the Soviet Union and other studies from Eastern countries claim a number of adverse health effects such as headaches, fatigue, irritability and sexual impotency among 500 kV switchyard workers. However, studies by groups in Sweden and the U.S.A. reported no statistically significant difference observed between those workers who had been exposed to strong electric fields and those who had not. Recently studies in Canada[5] support the findings in the U.S.A. and Sweden. In all these studies, the

number of people investigated was small so that no reliable information can be inferred concerning health effects which have a low frequency of occurrence (e.g. mortality rates). Also, adverse effects with long dormant periods would not have been detected by the studies done so far. Finally, the actual exposure, of the people investigated, to electric fields is not known, since there has not been an electric field detector that makes continuous monitoring possible. For this reason, a device was desired which could provide continuous monitoring of electric field exposures. A survey of existing devices (all of which are based on induced current between two metal plates) shows that they have a number of disadvantages[6]. Firstly, most devices have directional dependent sensitivities and are adversely influenced by harmonic content of the applied field. Secondly, they are made of metal and thus create a hazard to workers using them because of the risk of flashover.

The initial motivation for the work described in this thesis was to develop a monitoring device which would not suffer from the effects cited above. It would then be possible to carry out better studies on the correlation between exposure to electric fields, and possible adverse health effects. However such a device would have other promising applications. For example, many crane operators have been killed (2 in B.C. last year) when the crane touches the powerline. Existing electric field detectors do not reliably warn operators of heavy construction equipment of the dangers posed by overhead transmission lines[7].

This Thesis describes the theoretical, experimental and engineering work done to develop a new electric field meter. The meter is based on a principle which is totally different from that of existing meters. The new meter is based on the electrical breakdown of a low pressure gas in an

insulating envelope. This phenomenon is known as electrodeless breakdown and during the course of developing the electric field meter, many new results were obtained concerning the physical processes occurring in electrodeless breakdown.

The remainder of the introduction describes the typical fields to be measured, the existing electric field meters and introduces the concept of the new electric field meter GEM (Gaseous Electric Field Meter).

Section 2 presents a review of the literature related to the effect on which GEM is based. Section 3 is devoted to a description of the Physical Model for GEM, it contains all the basic theory. The design of GEM, which contains the actual physical and engineering considerations, is given in Section 4. Section 5 is a detailed account of the major experimental results obtained in the laboratory and in preliminary field tests which form the experimental basis of Sections 3 and 4. Finally, Section 6 contains the conclusions and expected future developments.

1.1 Environmental Electric Fields

Environmental electric fields are due to the potential difference between energized conductors (powerlines) (typically 100V to 1000kV) and the ground (0v). The field's magnitude and direction depends on the number, distribution and voltage of the conductors, the ground cover, the environmental conditions and any objects present nearby.

Typical fields under 3 phase transmission lines are approximately elliptically polarized in a vertical plane. The major axis of the ellipse is nearly vertical due to the presence of the horizontal ground plane (electric fields are perpendicular to the surface of good conductors). The ellipse is a result of adding the fields from each phase. At an equal distance from each wire the actual fields cancel out to zero (a major property of three phase transmission). However, when the distances to each wire are not identical the resultant field does not vanish. Thus the magnitude of the electric field under a transmission line exhibits a two hump camel shape having a minimum near the center conductor (approximate cancellation) and a maximum near each outer conductor (least cancellation). A typical field is sketched below.

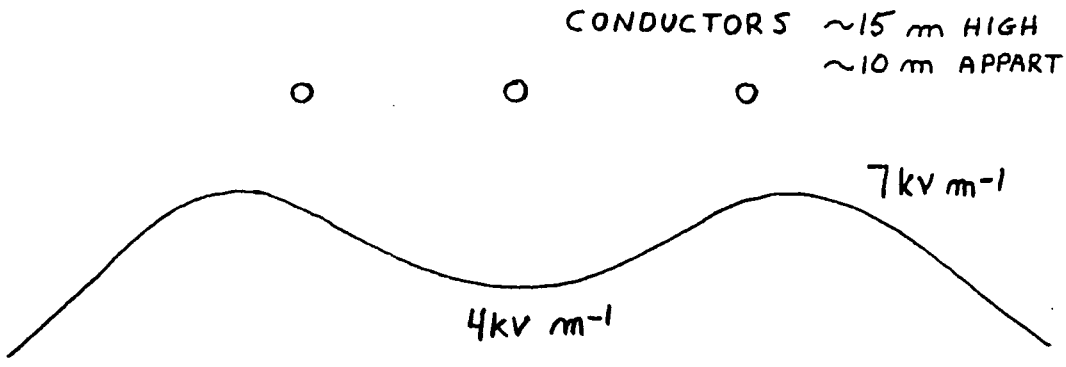

The field in a switchyard is much more complex due to a large number of powerlines of different voltages, heights and directions. However, the field at any given position is still elliptically polarized.

The description so far has ignored the presence of large conducting objects. These objects can severely distort the electric field lines . For example the field near the head of a person can be 10 times larger[8] than the ambient field in the absence of the person. This enhancement is due to a concentration of field lines near the head (see Figure 1).

An electric field meter must not only measure these complex fields but must operate in extremes of weather conditions (±40°C, 0 - 100% relative humidity) and extreme electrical noise (at 60 Hz and its harmonics).

Field around man standing in vertical electric field.

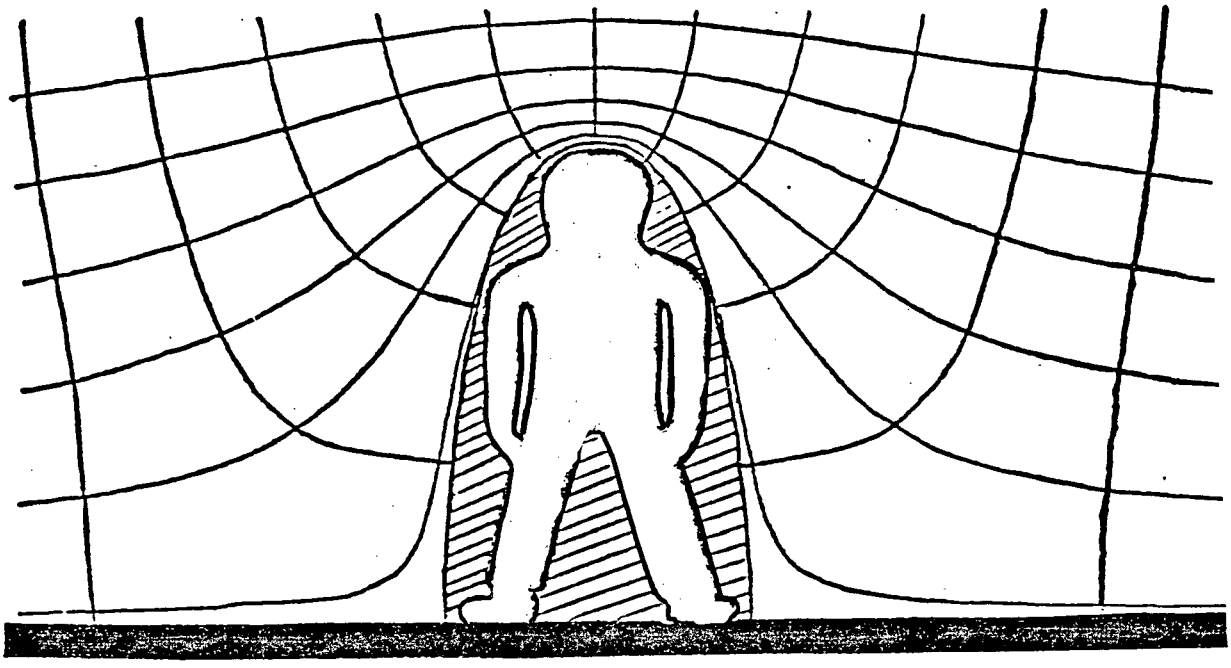

Field around stooped man.

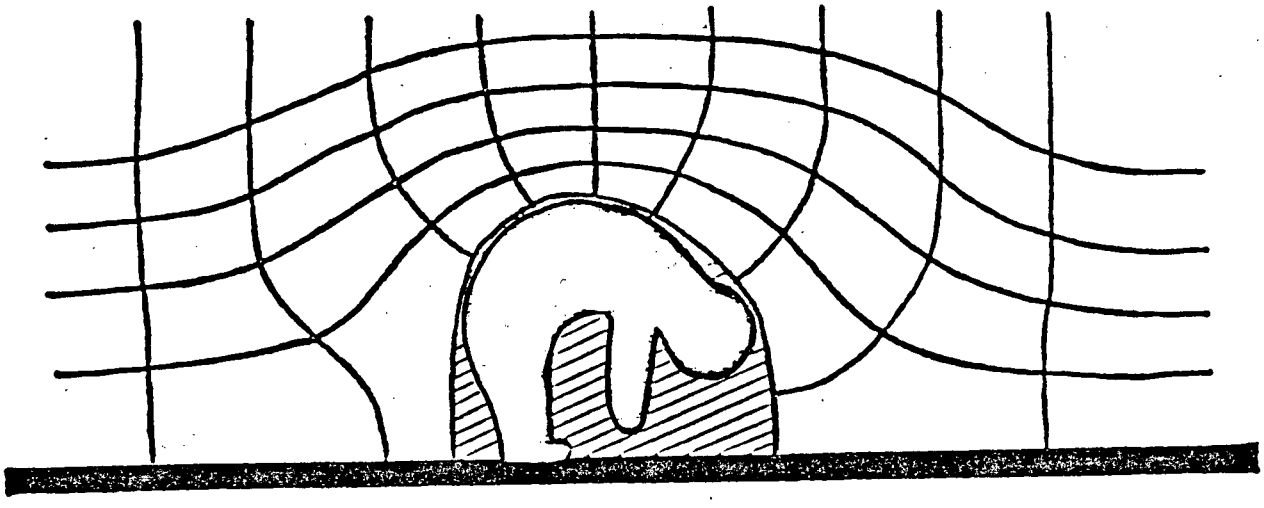

Figure 1 Equipotential lines surrounding human body immersed in uniform electric field (From reference 8).

1.2 Principle of Operation of Existing Electric Field Meters

Invariably present electric field meters consist of two metal halves separated by an insulator. When immersed in an electric field the field induces an alternating charge (or current) which is directly proportional to the magnitude of the sinusoidal field. The meters work by measuring a quantity proportional to the charges induced on the sensing electrodes (metal halves) or by measuring a quantity proportional to the current between the electrodes. In both cases the meters respond to the average value of the rectified signal, but are calibrated to read in rms (assuming a uniform sinusoidal field).

The calibration constant depends on the shape and size of the sensing electrodes as well as on the field geometry. Typically the electronics required to detect the signal from the electrode is housed between or inside the metal electrodes. The meters yield a maximum reading when aligned with the direction of the field and a minimum (close to zero) when perpendicular to the field.

These meters have the following favourable attributes:

1. many of the measurement standards have been developed for them;
2. they can be miniaturized to the size of a cigarette box. However, if a readout is required (rather than just storage of the electric field reading at definite time intervals) wires (or an optical fiber link) must be used to connect the device to the readout meter.

The meters have the following disadvantages:

1. they are metallic and therefore dangerous because of the risk of flash-over from the high voltage equipment to the sensor;

2. they are directionally sensitive (ie. the sensitivity depends on the orientation of the device in the electric field);
3. because the output is proportional to the average rectified signal the presence of harmonics in the electric field introduces an error which depends on the amplitude of the harmonic components. The error also varies with the phase difference between the harmonics and the fundamental;
4. they are made of metal which greatly perturbs the field and thus a meter calibrated in a unform field may not be accurate in a non-uniform field;
5. a self contained meter (ie. one in which the electronics and display are together with the sensing electrodes) is heavy;
6. a meter in which the display electronics and the sensing electrodes are separated (for example meters for cranes) is susceptible to electrical noise because of the connecting metallic wires. If the two parts are separated by an optical fiber[9] the electronics with the sensing electrodes becomes more complicated and requires its own battery or power source (to modulate the light emitting diode).

Environmental effects of temperature and humidity on these meters are not well documented. However one study[16] shows that there are no adverse effects for temperatures from 0° to 40°C (information is not given for temperatures below zero). Over the temperature range of 0 to 40°C varying humidity was also found to have no adverse effect.

1.3 Possibilities for a New Electric Field Meter

An electric field meter is made of two parts:

1. the sensor which responds with a signal proportional to the electric field and
2. the detector which detects, amplifies and displays (or stores) the signal.

As can be seen some of the present meters combine the sensor and detector into one package. However others (mostly for use as warning devices) separate the sensor and detector. Typically (with one exception[9]) the link is a wire.

A new meter which overcomes the main disadvantages (metallic sensor, directional sensitivity, noise sensitivity, etc.) is desired. One of the main disadvantages, directional sensitivity, can theoretically be overcome. Three of the available sensors can be placed in three orthogonal directions. However these sensors influence each other (because they distort the field lines) unless they are separated by 2 or 3 sensor dimensions. Directional independence can also be overcome by using a non metallic isotropically shaped sensor. The non metallic sensor also reduces flashover risk and affords the prospect of greatly reducing the coupling of electrical noise from the sensor to the detector. A sensor of symmetrical shape without metal parts therefore becomes the main design objective. The need to measure and quantify the signal from the sensor with a detector which necessarily employs electrical components dictates another objective. The sensor and detector must be separated from each other by a signal transmission system which is immune to electrical noise, and which does not adversely

affect the sensor's performance (ie. does not distort the field). In practice a sensor which measures the component of the electric field along a specified axis and gives a maximum response when the preferred axis of the sensor is aligned with the field is highly desirable for many applications. For example accurate mapping of electric fields for research purposes or for the manufacture of electrical equipment. Thus the ideal sensor should be available with spatially isotropic or nonisotropic sensitivity.

Of the many phenomena that occur in the presence of electric fields, the emission of light by insulating solids and gases is most promising. A sensor based on this phenomenon involves no metal, can be made of any shape (spherical for isotropic response) and emits a signal (electromagnetic radiation) which can be transmported to the detector by an insulating optical link.

Initial experiments carried out by exposing electrodeless glass bulbs filled with neon to alternating electric fields revealed that the bulbs emit intense pulses of light. The number of pulses per second was proportional to the strength of the applied field while the pulse amplitude did not seem important. The fact that the information is contained in the number of pulses gives the meter as a whole the advantage of being a digital system, therefore making the design of the detector simple and noise immune.

In conclusion, to measure the complex environmental electric fields with maximum accuracy and minimum danger (to the person using it) a new meter with a non metallic sensor is required. The meter can be based on the breakdown of gases in electrodeless glass vessels. The next section discusses work on electrodeless breakdown of gases done by others prior to the development of the GEM.

2.0 Existing Work Related to Electrodeless Breakdown

The breakdown of gases by electric fields in fluorescent lighting and neon signs is a familiar sight. However in all these cases metal electrodes are in contact with the gas. Electrodeless breakdown occurs when the electrodes that generate the field (the high voltage lines in this case) are separated from the gas by an insulating vessel. The physics of this type of breakdown is totally different, mostly because the electrodes and the gas (which becomes a conducting plasma after breakdown) cannot form an electrical circuit. Instead the vessel walls play a major role. Depending on the frequency of the applied field electrodeless breakdown takes different forms[10]. At low frequencies (less than 100Hz) discharge occurs as current pulses almost independently in each half cycle. The discharge is governed by primary and secondary processes as in D.C. breakdown. The vessel walls play a dominant role in the discharge. As the frequency is increased, products of the discharge in one half cycle remain to assist the subsequent discharges, and a decrease in threshold field (field below which the gas will not breakdown) results. At even higher frequencies the electrons are swept a shorter distance in each half cycle: when their oscillation amplitude becomes less than the length of the vessel, the walls no longer play a dominant role, the discharge becomes continuous and the breakdown threshold decreases. Eventually at very high frequencies the electrons stop colliding with the gas molecules and the discharge threshold increases rapidly.

The high frequency regime has been studied because of its application to plasma display panels. However, the low frequency regime

received attention for a brief period during the 1950's and then quickly disappeared even from many well known text books. In fact the preliminary work on GEM was done without knowledge of the published results.

Harries and von Engel[11, 12, 13] did most of the work on electrodeless breakdown at 50Hz. One of their main motivations was to understand the breakdown of insulation used in electrical equipment (insulation develops small air pockets in which electrodeless breakdown occurs and eventually destroys the insulation). They studied the breakdown mechanism by observing the current pulses produced with each discharge. This work lead to the basic explanation of why current pulses occur. However they did not study the light emission during breakdown, nor did they correlate the current or light pulses to the applied electric field to derive a measure of the field. Their work was also done only with uniform single phase sinusoidal fields in the laboratory. It also did not concern itself with vessels of different shapes nor with the interaction of on-going discharges with the vessel walls.

The theory behind the operation of GEM is described in the next section in terms of a physical model for the sensor. The physical model has its starting point on the work on D.C. breakdown and on Harries' and von Engels' work.

3.0 Physical Model

3.1 Introduction

The physical model for GEM is a theoretical approximation to the sensor used to explain and understand how the sensor works. The model is based on the literature (see Section 2) and numerous new experiments carried out during the development of GEM (see Section 5).

There are many practical (engineering) reasons to develop a physical model:

1. it allows a deeper understanding of the basic phenomena and therefore the theoretical advantages and limitations of the device;
2. it sheds light on methods of controlling major meter parameters (such as threshold and response to environmental effects) and
3. it allows prediction of results which are hard to obtain experimentally (such as the influence of harmonics).

This section will describe the basic breakdown phenomena for homogeneous linear fields first. Results will then be extended to plane or rotating fields (ie. more typical environmental fields). Practical considerations such as environmental effects, harmonics and meter design are deferred to Section 4.

3.2 The Breakdown Mechanism

As stated previously the breakdown mechanism at low frequencies is the same as D.C. The reason for this will become apparent in Subsection 3.3. Breakdown in D.C. fields is governed by the Townsend[14] mechanism which has been intensively studied because of the important role it plays in the formation of sparks between metal electrodes. Townsend formulated the following theory.

Consider N electrons propagating through a gas which is exposed to an electric field. The electrons are accelerated by the field and ionize atoms by collisions. The number of new electrons produced per unit distance $\frac{dN}{dx}$ is proportional to the number of electrons.

$$\frac{dN}{dx} = \alpha N$$

Where α , the constant of proportionality, is the first Townsend coefficient. Thus the number of new electrons (DN) after a distance d is given by

$$DN = No \ (e^{\alpha d} - 1)$$

Where No is the initial number of electrons.

Photons emitted by the excited atoms bombard the interior of the containing vessel and produce more electrons which can also contribute to the growth of ionization within the gas. Let the probability of secondary emission from the walls be γ (per electron from the primary

avalanche) where γ is known as the second Townsend coefficient. If an avalanche starts with one electron the number of secondary electrons after the first avalance will be

$$\gamma(e^{\alpha d} - 1)$$

If the process is continuous the number of electrons after many avalances will be

$$1 + \gamma(e^{\alpha d} - 1) + \gamma^2(e^{\alpha d} - 1)^2 + \ldots.$$

$$= \frac{1}{1 - \gamma(e^{\alpha d} - 1)}$$

Clearly all the gas in the container will be ionized if the denominator of the above expression vanishes, ie. if

$$\alpha d = \ln\left(1 + \frac{1}{\gamma}\right)$$

This expression is known as the Townsend breakdown criterion. The following important observations can be made:

1. α depends on the energy acquired by the electron per mean free path. The electron must acquire enough energy to ionize an atom, otherwise the number of electrons will not increase. Thus below a certain field α tends to 0 and the Townsend criteria cannot be satisfied. This field is the threshold field E_o for avalanche growth;

2. the dependence of the criterion on γ is logarithmic and therefore weak. γ is governed by the secondary emission material (ie. the vessel walls in this case) and
3. the dependance of the criterion on α is linear. α is therefore most important for threshold control.

Since γ is set by the secondary emitter surface it is constant for a given sensor material and geometry. Thus αd is constant. α is a function of the energy gained per mean free path ($E_o \lambda$)

$$\alpha = f \frac{(E_o \lambda)}{\lambda}$$

where λ is the mean free path and f the arbitrary function. It follows that

$$\frac{f (E_o \lambda)}{\lambda} \quad d = \text{constant}$$

or since λ = constant / p (gas pressure)

$$V_o = E_o d = \phi (pd) \qquad (1)$$

Where ϕ is another function, p is the gas pressure (related to λ) and V_o is the threshold voltage. This remarkable result is known as the Paschen Scaling Law. What equation (1) says is if p d is held constant and d is varied the threshold field E_o can be controlled (E_o varies inversely with d for constant pd). This is one of the two most important results in the construction of low threshold

sensors. The other consideration is the value of pd. The shape of $\emptyset$ can be deduced from the basic physics. At very low pressure there are almost no molecules and therefore a large voltage is required to start breakdown. At very high pressures there are so many collisions that a very high voltage is required in order for the electrons to gain sufficient energy. Thus $\emptyset$ must have a minimum somewhere between these two extremes. A graph of V_o versus pd resembles an asymmetric parabola. It is at this minimum pd that the sensor must be operated. Typically $\emptyset$ has a broad minimum near pd $\sim$ 10 to 60 Torr mm.

Table 1 shows typical values of the parameters discussed for different gases. Inert gases are highly desirable because of their long life (very stable, no chemical decomposition). Neon and Argon can be used because of their low V_o. Pyrex is the best choice for sensor material because of its availability, ease of use, toughness and value of γ not substantially worse than for other glasses.

gas	V_o (v)	pd minimum (Torr mm)
neon	230	4
argon	220	1.5
air	350	6.0

Table 1 a) Breakdown parameters for different gases

material	γ
pyrex	very low (less than 10^{-3})
metal electrode	0.01
photomultiplier coating	0.3

Table 1 b) Breakdown parameter for different materials

Table 1 Breakdown Parameters

3.3 Breakdown in Insulating Vessels

In a normal spark gap the breakdown starts as described in the previous subsection and continues as a steady discharge with the ionized gas (plasma) forming part of the electrical circuit. However in an insulating vessel the breakdown is interrupted by the vessel walls. Thus in a D.C. field one breakdown occurs, the charges separate and an internal field which cancels the applied field is set up. Instead of a continuous discharge there is one small pulse discharge.

The following discussion develops the model for an alternating linear field and spherical vessels with no conductivity. Clearly the orientation of the vessel with respect to the applied field does not matter. Suppose that a spatially uniform field $\underline{E}_A$, of fixed direction is applied and varies in time according to the expression

$$\underline{E}_A = \underline{E}'_A \sin \omega t$$

where E'_A is the amplitude of the field, t is the time and ω the frequency. In what follows the magnitude of electric fields is denoted by the appropriate symbol with the vector subscript omitted. Electrical breakdown will occur at high enough field strengths, and will evolve in accordance with the conventional Townsend Theory[14]. After breakdown the bulb is filled with partially ionized gas in which ions and electrons are separated by $\underline{E}_A$. The charge separation produces a space charge field, $\underline{E}_B$ which counteracts the effect of $\underline{E}_A$ (see Figure 2b). Since $\underline{E}_B$ is produced by the effects of the applied field, $\underline{E}_B$ is less than or equal to $\underline{E}_A$. If the conductivity of the partially ionized gas is large enough the

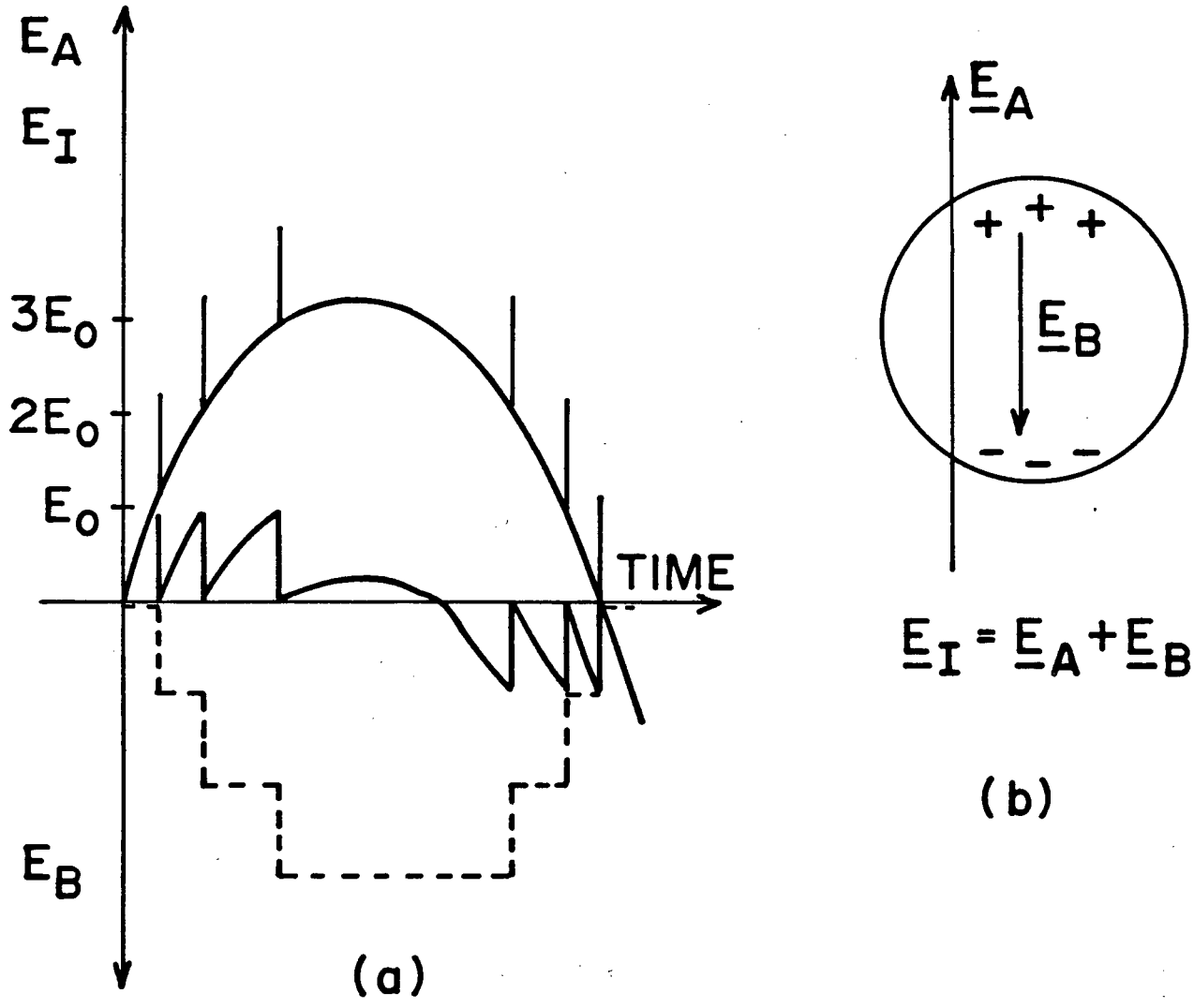

Figure 2 Field Strengths Applicable to the Bulb

a) Field strengths versus time.

E_A- sinusoidal applied field

(vertical lines are superposed optical pulses)

E_I- sawtooth internal field.

E_B- stepwave space charge field.

E_o- breakdown field strength.

b) Geometry of $\underline{E}_A$, $\underline{E}_B$ and $\underline{E}_I$

internal field, $\underline{E}_I$ is rapidly brought to zero[11] so that

$$\underline{E}_I = \underline{E}_A + \underline{E}_B = 0$$

If, however, the degree of ionization following breakdown is too low, the total separation of ions and electrons will produce a space charge field, $\underline{E}_B$, which is weaker than $\underline{E}_A$. Hence a residual internal field $\underline{E}_I$ will remain in the bulb, and will be in the same direction as $\underline{E}_A$. It is convenient to distinguish between these two cases by the terms 'strong breakdown' ($\underline{E}_I$ = 0 just after breakdown) and 'weak breakdown' ($\underline{E}_I$ greater than 0 after breakdown). One would expect large amplitude optical pulses to occur in strong breakdown, and lower amplitude pulses to arise from weak breakdown. The separated charges reside, between breakdowns, on the inner surface of the glass shell, where they are held in place by polarization forces. The charges are therefore immobile, and E_B can only be changed by subsequent breakdowns. The extra charges transported to the glass on such occasions either neutralize those already there, or increase their concentration[11-13].

3.3.1 Strong Breakdown

The evolution of the fields for strong breakdown is shown in Figure 1a. The applied field $\underline{E}_A$ has a sinusoidal waveform, and the vertical lines signify the occurrence of optical pulses. $\underline{E}_B$, which represents the space charge field in the bulb is the stepped waveform below the time axis. It is constant between optical pulses in accordance with the assumed immobility of charges adhering to the glass. $\underline{E}_I$, which is the

sum of $\underline{E}_A$ and $\underline{E}_B$ is the saw-tooth wave form. Each time that E_I reaches the breakdown field (E_o) of the gas in the bulb, a breakdown occurs, accompanied by a flash of light, and E_I is reset to zero. The process recurs when E_I again reaches a value of E_o. Changes in E_I between breakdown correspond to changes in E_A. Therefore the change in E_A between optical pulses is simply E_o(see Figure 2). Thus for strong breakdown the average number of pulses ($\bar{n}$) per cycle of the applied field is given by the expression[15]

$$\bar{n} = 2[2E_A'/E_o]$$

where the square brackets denote the integer part of the ratio $2E_A'/E_o$. If the frequency of the applied field is f_A then the frequency (f_B) of the optical pulses is given by the expression

$$f_B = 2[2E_A'/E_o]f_A \qquad (2)$$

Thus f_B depends in a stepwise fashion on E_A' (solid line in Figure 3)

A step occurs each time tha E_A' increases by $E_o'/2$, where E_o' is the average breakdown field of the gas. The step in the pulse frequency has a size of 2 f_A (see Figure 3). Since, in strong breakdown the conditions inside the bulb are identical for the production of each successive pulse, one would also expect much less variation in pulse amplitude for strong breakdown than for weak breakdown.

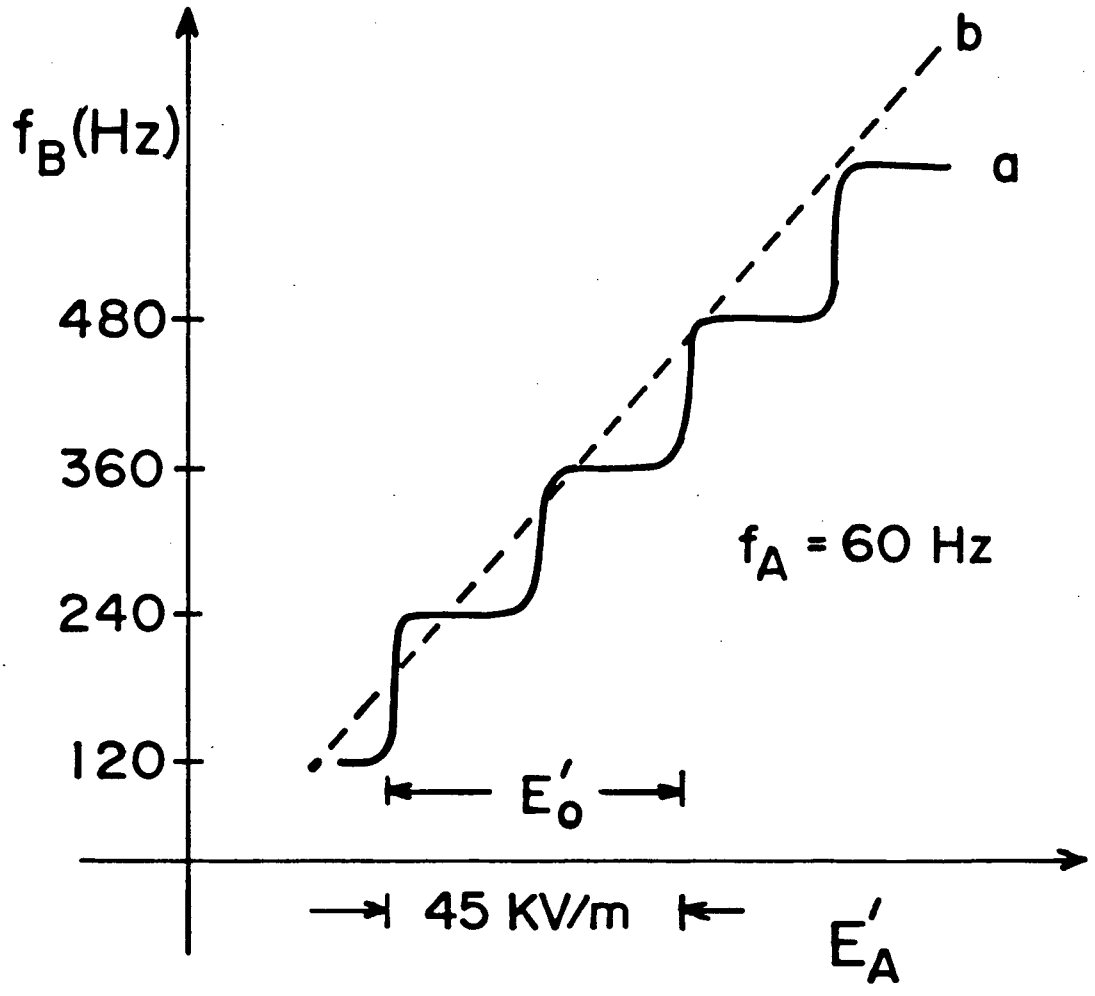

Figure 3 Frequency (f_B) of the optical pulses versus applied field amplitude (E'_A) for 25mm diameter bulb.

a) High pressure neon (10 Torr)

b) Low pressure neon (1 Torr)

3.3.2 Weak Breakdown

In weak breakdowns, E_I is not reset to zero by a breakdown. Hence the change in the applied field required to make the internal field (E_I) equal to the breakdown field is smaller than E_o. Because of the statistical fluctuations in E_I from one optical pulse to the next, it is to be expected that the step exhibited in Figure 3 will be smoothed out, and that to a good approximation f_B will depend linearly on E_A' (dotted line in Figure 3). It is also to be anticipated that the change in E_A between optical pulses will be smaller, the weaker the pulses. This effect is illustrated in Figure 4 which shows the optical pulses superposed on the applied field waveform for weak breakdown.

3.3.3 Start-up Conditions

The minimum field strength required to maintain steady state operation of the bulb is $E_A' = E_o/2$ (equation 2). It would appear that a field of strength $E_A' = E_o/2$ is too small to intiate this regime because it has been assumed that the gas has a breakdown field of E_o. However if one waits long enough the statistical properties of the phenomenon ensure that the first breakdown occurs even when E_A' is less than E_o. This is particularly true in the weak breakdown regime.

3.3.4 The Penning Effect

The value of the breakdown field E_o is governed by the Paschen law. In the case of simple inert gases such as Ar and Ne the threshold is set

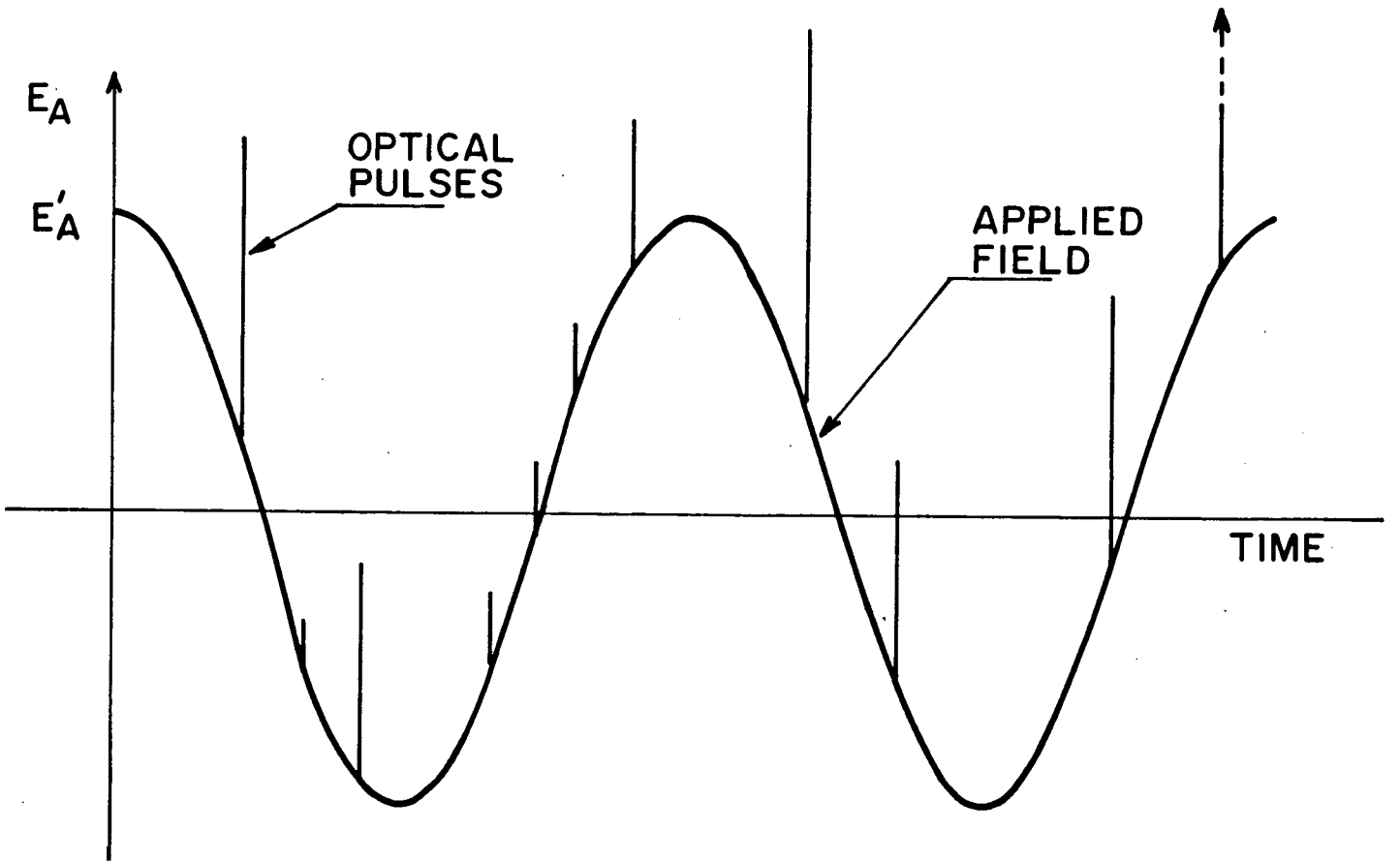

Figure 4 Optical pulses superposed on applied field wave form (E_A) for 25mm diameter neon-filled bulb at 1 Torr (weak breakdown case). E'_A = field amplitude.

by V_o/d. One of the drawbacks of GEM is that E_o, for a given gas, can only be decreased by making larger and larger sensors (which is not desirable) Thus it is important to consider ways of lowering Vo. The Penning effect is such a possibility. When a mixture of gases is used (say Ar and Ne) and the majority constituent has metastable states (99% Ne) then the threshold for breakdown can be lowered. This happens because the metastables retain the energy put into them and ionize more of the minority gas atoms provided the excitation energy of the gas metastable level exceeds the ionization energy of the minority component of the gas mixture. The net effect is that more electrons are used for ionization (ie. α is raised).

Other possibilities for lowering the threshold include doping the inert gas with a small percentage of radioactive gas (say tritium). The radioactive emissions collide with the atoms and provide more "seed" electrons from which avalanches can grow.

3.3.5 Finite Conductivity Effects

The models presented above depend on the assumption that the bulb has zero electrical conductivity. If the conductivity is finite, then the gas is exposed to a field E_T, which is different from E_A (see Appendix I*). However, the model remains valid provided E_A is replaced by E_T. At low frequencies severe screening occurs and the bulb ceases to produce optical pulses. At higher frequencies the field (E_T) which

* Appendix I was developed by F.L. Curzon.

penetrates the glass is phase shifted but not attenuated significantly. This means that graphs of E_A versus time can be converted into plots of E_T versus time by slightly displacing the curves to the left. Drastic increases in electrical conductivity can be produced by high humidity or high temperature. Therefore in these conditions the bulb may cease to operate.

3.4 Breakdown guided by the Vessel Walls (linear fields)[16]

3.4.1 Introduction

So far the discussion has dealt with vessels whose walls do not interact with the evolving discharge. The walls only provide photo-electrons, stop the discharge and trap the charges. This picture is accurate as long as the vessel is spherical or cylindrical and aligned with the field direction. However in attempting to build a cylindrical sensor (for those applications which require the measurement of electric field components ie. directional sensitivity) one must treat the case in which the discharge interacts with the container walls as it travels from one end of the vessel to the other. This interaction must occur when the cylindrical vessel is at an angle to the electric field. A similar interaction must also occur in all vessels when complex rotating fields are present.

In the following subsections the physical model is evolved for the case depicted in Figure 5. A cylindrical vessel at an angle θ with the applied field. First two possible physical effects that may govern the discharge are introduced. Then each effect is discussed independently.

3.4.2 Possible Effects

Free electrons which intiate discharges move along electric field lines. As seen in Figure 5 these lines are vertical (direction of E_A) and thus one would expect the electrons to move in a vertical direction

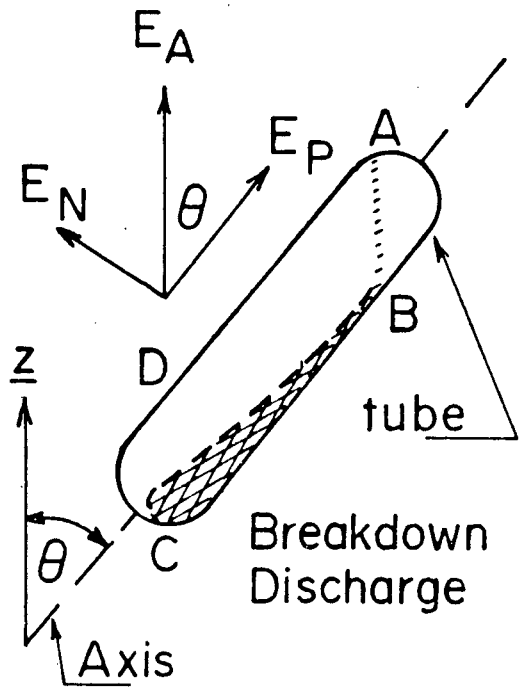

Figure 5 Geometry of applied field and breakdown discharge.

E_A = applied field; E_p = field along tube-axis;

E_N = field normal to tube-axis; θ = angle between tube axis and vertical (z).

Shaded region - breakdown discharge with internal field along z.

until they hit the vessel walls. If the electrons stick to the wall as soon as they hit it then there will be no breakdown, at least in the case of very narrow tubes. However, Harries, based on his work, believes that many collisions are required before electrons will stick. Thus one possible mechanism is for the tube walls to "guide" the discharge from one end of the tube (C in Figure 5) to the other (A). Another way in which the electrons may travel from one end of the tube to the other is if the internal field (inside the vessel) is parallel to the tube axis. The applied field, E_A, has two components (see Figure 5): E_N, normal to the tube and E_p, parallel to the tube. Suppose that E_N is screened by some mechanism but E_p is not, then the discharge will proceed along E_p.

In conclusion, if a discharge is to proceed from one end of the tube to the other either the normal component of the applied field is screened or the tube walls guide the discharge. The next two subsections describe these models.

3.4.2.1 Finite Conductivity Screening

The screening due to the finite conductivity of the glass varies inversely proportional (for a given glass surface condition) with the vessel dimension. A small vessel will screen the field more than a large vessel. Thus it may be possible in a narrow tube for E_N to be screened while E_p is not.

If this is the case then the gas will behave as if it were immersed in an axial field of strength

$$E_p = E_A \cos \theta$$

and will yield a corresponding value of breakdown frequency (ie. equation 2 with E'_A replaced by E_p). Clearly when θ is 90° there are no pulses.

3.4.2.2 Wall Collision Guidance

Now assume that finite conductivity is not responsible for the effect. Furthermore assume that electrons are accelerated towards the vessel walls bounce off and are again accelerated. If during the wall collision almost no energy is lost then the electrons will be guided to the other end of the tube. The effective energy gained by then will be

$$E_A \quad L \quad \cos \theta$$

where L is the length of the tube (assuming the width direction is very small). This expression is simply the potential difference between the ends of an inclined tube. Thus an inclined tube is equivalent to a tube aligned with the field of length L_e (assuming the tube is infinitely thin)

$$L_e = L \cos \theta \qquad (3)$$

Experimental results presented in Section 5 show that this model is correct. Thus the frequency of breakdown in electrodeless tubes is governed by the potential difference between the ends of the tube, provided the discharge is guided by the tube walls. A thin cylindrical tube therefore measures the component of the electric field along its axis (ie. produces a maximum reading when aligned with the field).

3.4.2.3 Extension to Cylinders of Finite Width

If the cylindrical tube has a width which is a significant fraction of its length, then the model is complicated. Basically, the effective length is no longer

$$L \cos \theta$$

but includes a term proportional to the width of the tube. Furthermore the maximum reading is most likely at a small angle from alignment with the field (ie. along the largest path or diagonal of the tube). "Fat" tubes are not treated in any more detail because they do not have any obvious application.

3.5 Breakdown In Planar Rotating Fields[17]

3.5.1 Introduction

The physical model developed so far has considered only spatially uniform electric fields of fixed direction (linear fields). The model, however, is applicable to non uniform fields provided the sensor dimensions are smaller than the length scale of the non uniformity. This is usually the case. Environmental electric fields are typically planar rotating (in an elliptical envelope, see Section 1.1) and thus the physical model must be extended. However, it should be mentioned that in many applications the electric field meter is placed near a large conducting object (ie. person, crane, etc.) where to a good approximation, the field is in a fixed direction (ie. perpendicular to the objects surface) and uniform over a scale a few times smaller than the objects radius of curvature.

The following subsections will discuss the model for spherical and cylindrical vessels in plane circularly polarized fields. The results will then be extended to plane elliptically polarized fields.

3.5.2 Breakdown in Circularly Polarized Fields

A circularly polarized field has a constant magnitude E_A but rotates at a constant rate (60 Hz) in the plane of polarization. Any projection of this field is the familiar spatially uniform field in a fixed direction.

3.5.2.1 Cylindrical Tubes

The extension of the physical model for cylindrical tubes to planar rotating fields is simple. Cylindrical tubes measure mainly the component of the electric field along the tube axis (see Section 2.4.2.2) irrespective of whether the field is planar rotating or not.

Due to the finite aspect ratio of the cylinder, the direction of the measured component is in error by roughly $\pm 2^0$ for a typical tube (length, 55 mm, diameter 4 mm). The cylinder responds only to E_p (the component of the field along the tube), if the following condition is satisfied

$$E_N < (L/D)E_o$$

where E_N is the field component perpendicular to the cylinder axis, L is length of the cylinder and D its diameter. This condition means that E_N is not strong enough to cause a breakdown across the tube. For a typical cylinder (L = 50 mm, D = 4 mm), E_N can be twelve times as large as the axial breakdown field before it influences the response of the bulb. If E_N exceeds LE_o/D, then it is convenient to define a rejection ratio r, by the expression

$$r = 1 - \hat{E}_p/\hat{E}_N$$

where $\hat{E}_p$ and $\hat{E}_N$ are the respective parallel and perpendicular field components required to produce a given f_B. It is readily shown that

$r = 1 - (D/L)$, which for a typical cylindrical bulb, has the value, 0.9. Thus in a circularly polarized field of magnitude E_A ($E_A < L/D\ E_o$) the cylindrical tube measures E_A as in equation 2, where E_o is governed by the full length (L) of the cylinder. The measurement is the same irrespective of orientation.

3.5.2.2 Spherical Bulbs

For spherical bulbs the extension of the physical model is more complex. Assuming the basic phenomena (Section 2.3) remains the same and that the internal field E_B in the bulb caused by the charge separation is uniform (this assumption will be discussed later), then a new breakdown still occurs every time the applied field changes by E_o, however the addition of the fields is now vectorial. For breakdown one must have

$$| \underline{E}_A + \underline{E}_B | = E_o$$

where the straight brackets indiciates the magnitude of the vectorial sum. In the special case where $\underline{E}_A$ is circularly polarized and $\underline{E}_B$ is uniform it is easily seen from Figure 6 that for the field to change by E_o, E_A must rotate through an angle θ given by

$$E_o^2 = E_A^2 \quad [(1 - \cos\theta)^2 + \sin\theta^2]$$

or

$$\cos\theta = 1 - \frac{1}{2}\frac{E_o^2}{E_A^2}$$

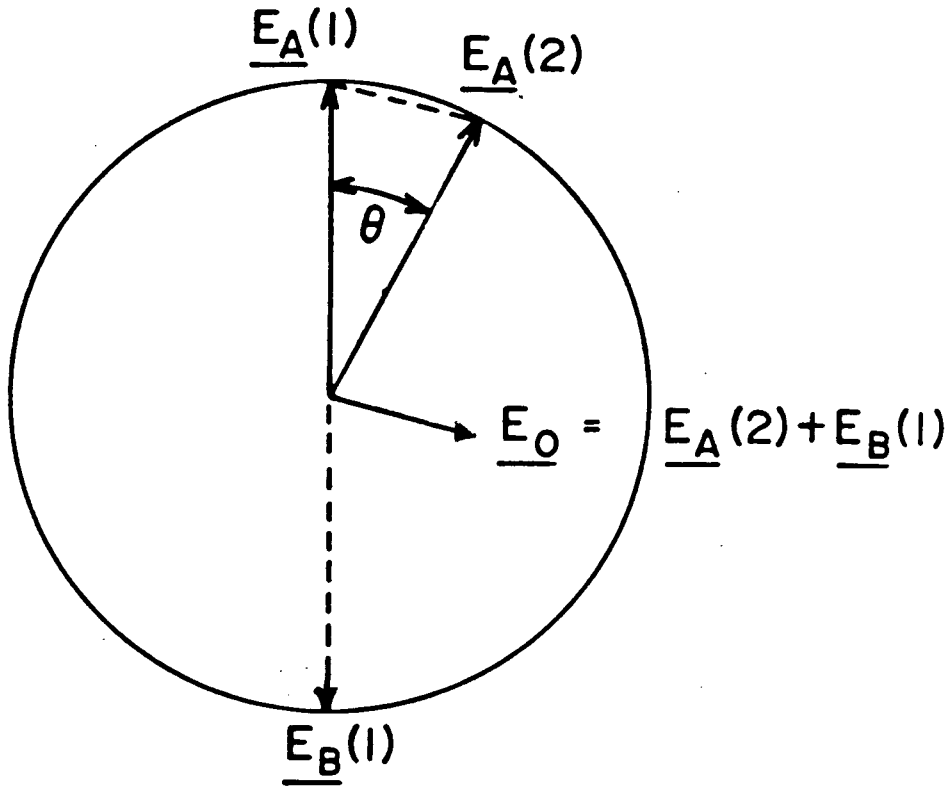

Figure 6 Geometry of Rotating Applied Field.

$\underline{E}_A(1)$ - applied field at 1st breakdown.

$\underline{E}_B(1)$ - "wall charge" field, 1st breakdown.

$\underline{E}_A(2)$ - applied field at 2nd breakdown.

$\underline{E}_O$ = breakdown field

Thus equation 2 which expressed the frequency of breakdown becomes

$$f_B = f_A \frac{2\pi}{\theta} = f_A \frac{2\pi}{\cos^{-1}\left(1 - \frac{1}{2}\frac{Eo^2}{E_A^2}\right)} \qquad (4)$$

Two important observations can be made concerning the calibration curve (f_B versus E_A):

1. the steps associated with strong breakdown have disappeared. This effect can be understood intuitively. The steps in the previous case were due to the fact that the change in $\underline{E_A}$ changes in sign. In one cycle $\underline{E_A}$ increases and then decreases. Steps occur because any increase in E_A of less than E_o followed by a decrease will not lead to a pulse (ie. near the peaks of the sine wave). In this case E_A is constant and changes in $\underline{E_A}$ due to rotation are always of the same sign and therefore there are no discontinuities (integer brackets) in equation 4 .
2. The number of pulses per second f_B for a given field amplitude E_A is increased by rotating the field except at threshold. This is apparent from equation 4. At threshold,

$$E_A = \frac{Eo}{2} \quad ,$$

the number of pulses is f_A as is also obtained with equation 2. However, for E_A larger than threshold equation 4 always gives a bigger value. For example for E_A much larger than E_o (well above threshold) θ approaches E_o/E_A and equation 4 becomes

$$f_A = \frac{2}{2}\frac{\pi}{}\frac{2E_A}{E_o}$$

Thus (neglecting the presence of steps) the number of pulses is enchanced by $\pi/2$ (1/4 the circumference of the circle). The actual enhancement factor varies slowly from 1 to $\pi/2$ as E_A is increased.

Now consider the case of E_B not uniform. Clearly this is the case in real life since E_B is formed by localized charges at the ends of the bulb. However in the case where $\underline{E}_A$ and $\underline{E}_B$ are aligned the non uniformity of $\underline{E}_B$ should have little effect on the physical model. This is why the non uniformity of $\underline{E}_B$ was neglected up to this section. When $\underline{E}_B$ is not uniform the condition for breakdown becomes

$$|\langle \underline{E}_A + \underline{E}_B \rangle| = E_o \qquad (5)$$

where the angular brackets indicate some form of spatial average of the vector sum over the volume of the bulb. The average is required because the breakdown condition depends on the field geometry (since E_B is not uniform). Equation 5 is very complex to solve and will not be treated further here. Qualitively two observations can be made

1. for large applied field (E_A much greater than E_o) the non uniformity of E_B can be neglected and previous results apply. This is because in this regime E_A and E_B are approximately aligned;
2. for E_A near threshold the non uniformity of E_B can play a significant role and must change the count rate given by equation 4.

3.5.3 Extension to Elliptically Polarized Fields

Elliptically polarized fields are like circularly polarized fields except that as $\underline{E_A}$ rotates it changes magnitude. At one extreme (constant E_A) these fields reduce to the circularly polarized fields, and the other extreme (very narrow ellipse) they reduce to the uniform fields in a single direction. Thus the effects expected for elliptically polarized fields lie somewhere in between.

In this section the symbol E_A will be used to denote the semimajor axis of the ellipse. This non standard use of E_A is desirable because the equations for the linear fields case carry over to this elliptical case.

In the case of cylindrical tubes there is no change. The tubes measure mainly the component of the field and will thus give a maximum reading when aligned with the semi major axis of the ellipse.

In the case of spherical bulbs circularly polarized fields cause two changes to the physical model: enchancement in the number of pulses per second for a given field magnitude and smoothing out of the steps. These effects also occur in elliptically polarized fields. The derivation of the pulse frequency f_B in elliptically polarized fields proceeds in a similar manner as the derivation of equation 4 (assuming E_B is uniform) and is treated in detail in Appendix II*. By analogy the result yields two effects

1. an enhancement** in the pulse frequency ranging from 1 at

* Appendix II was developed by F.L. Curzon

** The enhancement is defined as the ratio of f_B in an elliptical field of semimajor axis E_A' to f_B in a linear field, E_A'

threshold to 1/4 the circumference of the ellipse divided by E_A at fields high above threshold ie.

$$\theta = E_o/E'_A$$

and

$$f_B = f_A \quad \frac{\text{circumference}}{\theta}$$

2. A disappearance of the steps of f_B vs E'_A at fields high above threshold. In the circularly polarized fields the steps disappear because the change in E_A is always of the same sign. This is still the case in elliptically polarized fields if the semiminor axis field of the ellipse is larger than breakdown field. Otherwise steps will still be visible.

Thus very qualitatively the bulb behaves as in a uniform field when E_o is larger than the semi minor axis and as in a circularly polarized field (except that the enhancement is 1/4 the circumference of the ellipse divided by E'_A ie. less than $\pi/2$) when the semi minor axis field is greater than E_o. Non uniform effects of E_B also change the count rate for fields near threshold.

In conclusion:

1. Cylindrical bulbs measure the component of a planar rotating fields along the cylinder axis. As such they can be used, fully to characterize the field in space and time provided one orients the bulb in different directions and maps the field.

2. Spherical bulbs measure an "average" of the planar rotating field. This average is heavily dependent on the field geometry and magnitude. Because of this and spatially non uniform E_B effects the bulb must be calibrated for any given field geometry if accurate measurements are to be made (this is also the case with existing meters). On the other hand the measurement is independent of the orientation of the bulb with respect to the field.

3.6 Summary

When an electrodeless gas filled bulb is immersed in a spatially uniform field of fixed direction and magnitude (E_A') light pulses are emmited with a frequency

$$f_B = 2[2\ E_A'/E_o]\ f_A \qquad (2)$$

where f_A is the frequency of the applied field and E_o is the breakdown field of the gas. E_o is given by the Paschen Law

$$E_o = \emptyset\ \frac{(pd)}{d} \qquad (1)$$

where is a function with a broad minimum, p is the gas pressure and d the dimension of the vessel (the diameter for a sphere and the length for a cylinder). E_o can be controlled by the gas type and the dimension of the vessel.

A cylindrical tube immersed at an angle θ to the field still obeys (2) however the effective field is $E_A' \cos\theta$ not E_A'.

In planar rotating fields equation 2 must be modified. For cylindrical tubes E_A' must be replaced by the component of the field along the tube axis. For spherical bulbs the count rate is always larger than or equal to f_B given by equation 2 . The enhancement at very large fields is equal to 1/4 of the circumference of the ellipse divided by E_A'. Also at high fields (or lower fields for fat ellipses) the steps (integer brackets in equation 4) disappear.

The physical model presented so far has dealt with the basic ideal physics of the sensor in a controlled laboratory environment. The next section describes the full meter (sensor and detector) and discusses environmental effects especially on the sensor. Experiments confirming the predictions in this section and the following are discussed in Section 5.

4.0 Electric Field Meter Design

4.1 Introduction

This section describes a complete meter for measuring low frequency electric fields, specifically typical fields encountered under high voltage transmission lines and in substations. The meter is based on the application of the breakdown of gases in dielectric envelopes. A glass bulb filled with a gas (the sensor) emits pulses of light when exposed to the electric field. The number of pulses per second is a measure of the electric field. Since the device depends on electrical breakdown of a gas, it is referred to below by the acronym GEM (gaseous electric field meter).

The sensor has the following important properties. It contains no metal parts and can be made to have an isotropic or directional sensitivity. It provides information about the field strength by emitting light which is easily transported to a detector without the use of metal. Since the information is contained in the number of pulses emitted rather than in their height the output is ideally suited to digital processing. The above characteristics confer the following benefits on the field measuring meter. The meter is small, rugged and readily portable. It is accurate (better than 5%) and remains calibrated for periods of several months. Due to the output of light pulses from the sensor, the meter (detector + sensor) is easily shielded and operates well in noisy electrical environments. It is also safe to use and has good time resolution ($\sim$1 sec).

In what follows, the GEM and its parts are described. The description covers design aspects as well as practical considerations for meter operation in environmental electric fields.

4.2 Functional Description of the GEM[19]

The GEM is composed of three parts (see Figure 7): the sensor (lower left in Figure 7), which senses the electric field and generates pulses of light whose frequency is proportional to the field's magnitude; the optical fibre (upper part in Figure 7), which transmits the pulses of light to the detector, the detector (lower right in Figure 7), which counts the pulses of light and generates a digital reading proportional to the electric field magnitude. The output reading can be easily displayed to the users or stored for later retrieval.

The use of a long optical fibre (at least 2 m[8]) permits electrical fields to be measured undistorted by the presence of the person making the observation. A compact version of the GEM can be made by using a short fibre, or by mounting the bulb directly on the detector. However with such a system the field is disturbed by the user and by the presence of the detector. The following subsections describe each of the three parts in detail.

4.2.1 The Sensor

The sensor is a gas filled glass bulb enclosed in a protective dielectric case.

Figure 7 Photo showing prototype of instantaneous display unit (66% of real size).

4.2.1.1 The Bulb

The bulb is most easily made of pyrex (see Section 3.2) and filled with neon to a typical pressure of 1 torr for a bulb of 25 mm diameter (ie. Paschen minimum for neon). The shape of the bulb dictates its directional sensitivity. A spherical bulb (see Figure 8) is isotropic i.e., it gives the same reading irrespective of the field direction. A narrow cylindrical bulb, on the other hand, gives a maximum reading when the field direction is aligned with the axis of the cylinder. The bulb's electric field threshold is a function of the pressure and the length scale (L). For a spherical bulb L becomes the diameter while for a cylindrical bulb, L becomes the length of the cylinder axis. For a fixed product of pressure and length scale at the Paschen minimum the threshold field strength is inversely proportional to L. For example, a 25 mm bulb filled to 1 Torr has a threshold of 15 kV/m while a 38 mm bulb filled to 0.66 Torr has a threshold of 10 kV/m. In the weak breakdown regime the output pulse frequency is directly proportional to the electric field magnitude over broad ranges (10 to 60 kV/m) for low pressures (1 Torr). The sensor has a slight startup hysterisis. A field greater than threshold (typically 5% more (see Section 3.3)) is required to start it. However, once started, a reliable reading can be obtained in fields equal or higher than threshold.

4.2.2.1.1 Bulb Manufacture

To fill the bulbs with gas they are pumped down on a copper vacuum system by a 100 mm aperture diffusion pump equipped with a liquid

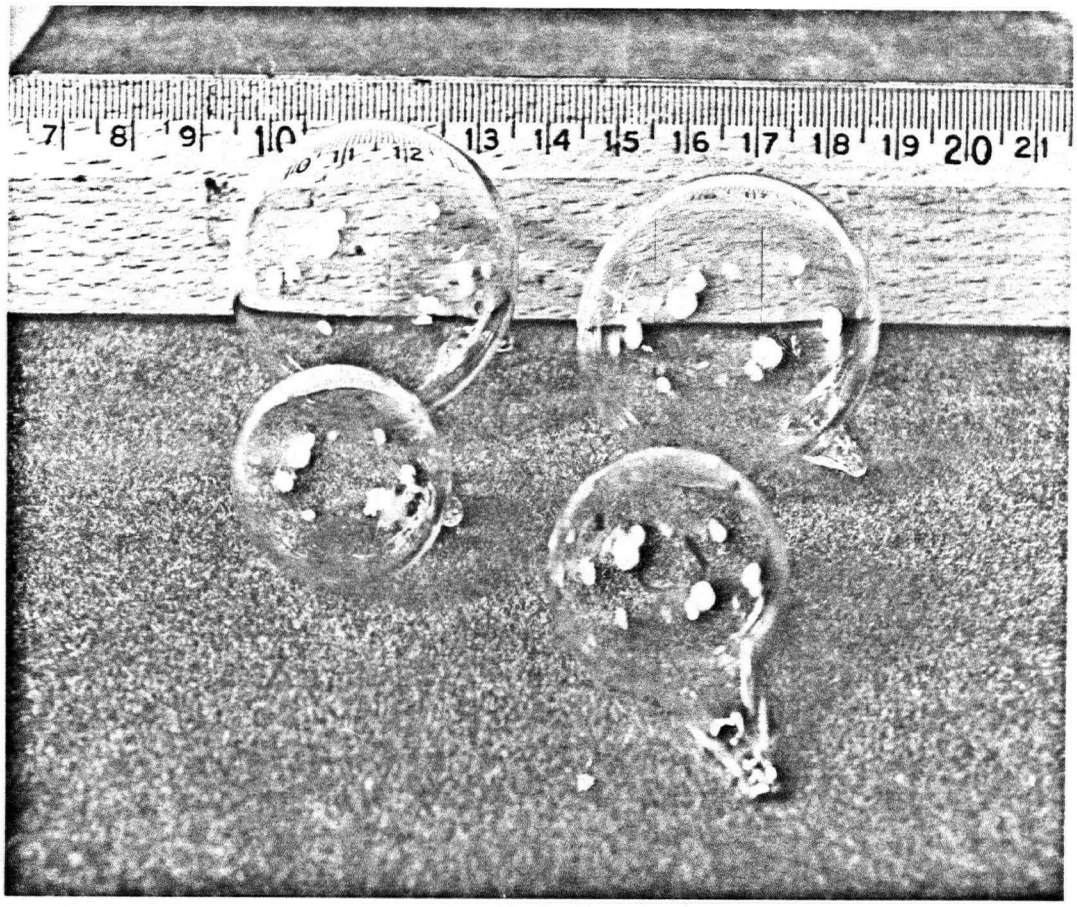

Figure 8 Photo showing typical bulbs.

nitrogen trap (Balzer's Diff 170, pumping speed 170 litres/sec). The diffusion pump is backed by a Sergent Welch rotary oil pump (Model Duoseal 1402, pumping speed 160 litres/min). The complete system has a base pressure of less than 5 x 10^{-6} Torr. After pumping for 24 hours, and baking at 280°C for 4 hours, the bulbs are filled to a suitable pressure with reagent grade gases, sealed, and then baked again at 280°C for another 4 hours. The second baking improves the performance of the bulbs, but it is not yet known why the improvement occurs.

Most of the bulbs have been made using neon (99.999% pure) and argon (99.9995% pure) obtained from the Matheson Co. In the neon, the chief impurities are helium (8ppm) and nitrogen (2ppm). In argon some impurities are present at the level of 0.1 ppm. Some bulbs have also been filled with commercially available dry air or nitrogen. The bulbs of the desired diameter, d, are filled to a pressure, p, such that pd is at the Paschen minimum (determined experimentally).

4.2.1.2 The Holder

The bulb is placed in a protective dielectric case, the holder. The holder serves three functions:

1. to protect the bulb from environmental conditions and handling;
2. to hold the optical fiber close to the bulb and allow the coupling of light pulses to the fiber and
3. to prevent most of the ambient light from entering the fiber.

The last two criteria can be met by most plastics. However the first criterion is more stringent. Glass increases its conductivity by

orders of magnitude when handled or exposed to large relative humidity[20] because mobile alkali ions can dissolve in adsorbed water. Thus for reliable operation the bulb must be enclosed in a container whose conductivity is not influenced by these effects. Teflon (polytetrafluorethylene) which is hydrophobic is the ideal material and has worked well in very humid environments. For more typical conditions (humidity under 70%) plexiglass (polymethylacrylate) is adequate. With these holders bulbs can be dropped from 2 m onto concrete floors with no damage.

4.2.1.2.1 Holder Manufacture

For research and test purposes holders are made by drilling out cylindrical stock of the desired material. The resulting cylinder with one closed end is capped with a screw-on cap of the same material. The fiber is fitted to the cap. In this manner the holder can be opened to replace the bulb.

Ambient light is reduced (it does not need to be eliminated because the electronics is sensitive to pulses not D.C. signals) by painting the holder black (inside) or by putting black electricians tape outside.

In production the holder will most likely be made by dipping the bulb (with the fiber glued to it) into molten holder material (say teflon).

4.2.1.3 Engineering Considerations

There are two types of practical considerations that apply to the sensor when operating in environmental fields: environmental effects (temperature and humidity) and the effects of field harmonics.

4.2.1.3.1 Humidity

As mentioned earlier humidity increases the conductivity of the glass and under extreme conditions can completely shield the gas from the field. The effect can be eliminated by protecting the bulb with a suitable holder.

4.2.1.3.2 Temperature

Temperature can have both direct and indirect effects on the performance of the sensor. Direct effects occur because the conductivity of the glass is increased with temperature and because the gas breakdown parameter changes with temperature. Both of these effects are minimal between -40°C and 40°C the typical operation range. Indirect effects are caused because temperature influences the concentration of materials adhering to the bulbs interior and exterior surface. The materials may be physically absorbed or chemically combined. On varying the temperature physical absorption is reversible whereas "chemisorption" is not. Absorption of material on the bulb surface has two effects:

1. it can influence glass properties such as conductivity or the secondary emission coefficient γ and

2. it can change the gas composition and therefore its breakdown properties.

To minimize these effects one must keep the bulb exterior clean and protected (by using the holder) and minimize the impurities inside the bulb. This is the main motivation for properly baking and pumping the bulbs during production as well as for using very pure gases. The extent of temperature effects must be evaluated experimentally. Results are presented in Section 5.

4.2.1.3.3 Harmonics[18]

The effect harmonics have on sensor operation depends on the shape of the sensor.

a) Cylindrical Tubes

Since a cylindrical tube responds only to the component of the field along its axis, it is only necessary to consider the effect of a linearly polarized field. The field will normally contain two major harmonic components: the fundamental (frequency, f_A, amplitude E'_A) and the third harmonic (frequency $3f_A$, amplitude E'_H). Typically $E'_H/E'_A < 0.1$. If $E'_H/E'_A < 1/9$ then the number of extrema in the field per cycle of the fundamental is not affected by the value of E'_H. The number of counts is therefore still determined by the largest value of the field strength, irrespective of the harmonic content.

b) Spherical Bulbs

The analysis for linearly polarized fields is identical to that given above. Hence the number of breakdowns per cycle of the fundamental component of the applied field is determined by the greatest field strength in the cycle. For elliptically polarized fields a typical phasor is shown in Figure 9. The enhancement in counts caused by the rotating field will be proportional to the circumference of the phasor, which, to first order in E'_H/E'_A is equal to the circumference of the phasor assuming no harmonic distortion ($E'_H = 0$). Thus as a first approximation the spherical bulb only responds to the fundamental component of the applied field. The largest field strength which can occur during the oscillation period of the fundamental is $E'_A + E'_H$. This field is therefore measured with a maximum fractional error of E'_H/E'_A.

4.2.2 The Fiber

The optical fibre is a commercial product purchased from Welch-Allyn. The prototype GEM uses a vinyl clad glass fibre bundle 2mm in diameter and 2 m long. Shorter or longer fibres can be used. Since the sensor light output is strong, a narrow fibre can be used and no special reflectors are needed to enhance the collection of light at the input to the fibre.

The most important property of the fibre cable is its conductivity which must be very low ($< 10^{-12}$ mho m^{-1} for typical fibres in fields of 60 Hz frequency). This property ensures that the field to which the sensor is exposed is not changed significantly by the fibre. Low

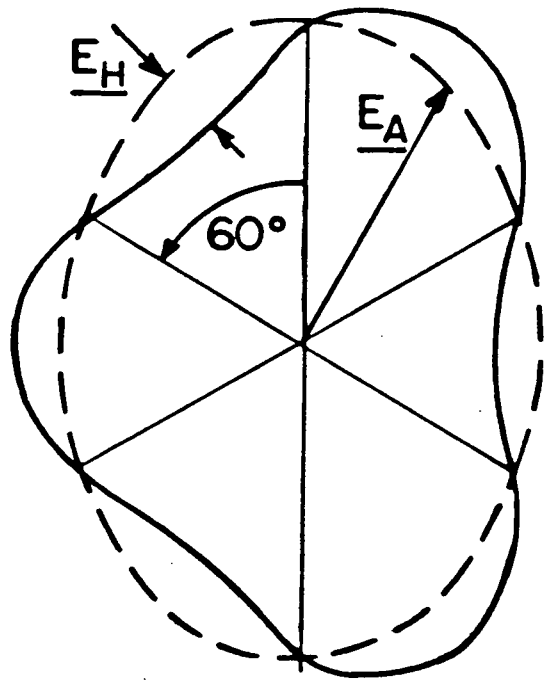

Figure 9 Phasors for Applied Field, $\underline{E_A}$

dotted curve - elliptical polarization - no harmonic distortion.

solid curve - elliptical polarization with 3rd harmonic distorition, $\underline{E_H}$.

conductivity also reduces the coupling of electrical noise from the fibre to the detector electronics. Many commercial fibre bundles are protected with a metal shield. These are obviously unsuitable. However, many of the fibres with no metal are coated with a conductive resin. In fact two sets of fibres supplied by the same manufacturer over a period of four months had widely different conductivities. The earlier set was satisfactory but the second set had unacceptably high conductivity.

Another important property of fibre bundle for this application is robustness. Continuous use of the fibre in the field can eventually lead to the breaking of some or all fibres in the bundle. This is only a problem near the end caps of the bundle where the flexible fibre bundle meets an inflexible cap. To overcome this problem the commercial fibre bundles have been re-inforced (near the caps only) with graded heat shrink tubing. This has the same effect as springs near the junctions between wires and electrical appliances.

4.2.3 The Detector

The detector is a small plastic box containing the electronics which are shielded by an internal metal sheet liner. The function of the detector is to measure the frequency of occurence of light pulses since this frequency is proportional to the electric field.

A simplified block diagram of the detector is shown in Figure 10. The photodetector detects the weak optical pulses which are then amplified and shaped. During this process all pulses whose amplitude is higher than a certain threshold (set above the noise level) are converted to standard pulses (same amplitude and duration). These pulses are then

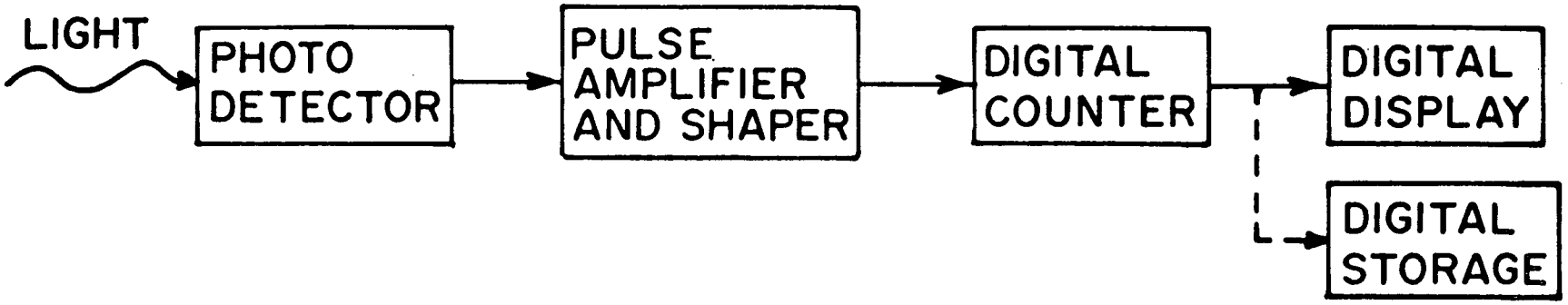

Figure 10 Block Diagram of Detector and Display System.

counted over a short time span (Δ t). After every period of length Δt the counter is reset to zero and allowed to count again. The longer Δt, the more accurate the reading, provided of course that the field does not change during this time span. The shorter Δt, the better the time resolution of the meter. A good compromise for typical alternating environmental fields is a time interval of one second. The fluctuation in the number of counts in each interval Δt tends to be constant, irrespective of the field strength. At threshold the error is typically 5% and correspondingly lower for stronger fields.

The counts which are directly proportional to the electric field can be either displayed to the user or stored for later retrieval. One lab prototype employs a liquid crystal display and has a rechargeable battery. The detector measures 110 x 60 x 30 mm and the batteries last for at least 10 hours (see Figure 7). Another lab prototype contains a microprocessor and some memory instead of the display. This prototype is slightly larger. In this case, for example, the minimum, maximum and average electric field reading every five minutes can be stored over an eight hour period. The electronics of both detectors are amenable to further minaturization.

4.2.3.1 Electrical Design

The detector electronics can be separated into two distinct parts (and boards). The first part which basically detects, amplifies and shapes the pulses is specific to this application. The second part which consists of a digital counter and display system is a very standard component of most digital devices and will not be described further.

The circuit diagram for the photodetector, amplifier and pulse shaper is shown in Figure 11. The circuit is made with standard off the shelf components (which can operate between -30°C and 40°C). Light is detected by a phototransistor (FPT100). The signal is fed through a low noise FET to a series of four operational amplifiers (all within a chip) for amplification. The total gain is about 30,000. Each amplifier stage is only A.C. coupled to the next stage (ie. capacitor followed by resistor at the input of each operational amplifier) in order to reduce low frequency noise. Finally the amplified voltage pulse is put through a comparator and converted to a standard height pulse. The threshold for the comparator can be adjusted with a variable resistor (R21) so as to detect only those signals which are above the noise level (ie. when the electric field is of). To reduce the 60 Hz noise further the power supply is decoupled as shown in the lower right of Figure 11.

The above design and the counter and display electronics can operate from a 9v rechargeable battery for 10 continuous hours.

It is possible to reduce the size of the detector if required for certain applications. For example the present circuit for the photodetector, amplifier and pulse shaper uses about four IC's. These could be combined into one chip. If desired the whole detector could be packaged in a 50 x 50 mm board (at a setup cost of less than $50,000).

4.2.4 Overall Engineering Considerations

Most of the engineering considerations apply to the sensor and have been discussed in Section 4.2.1.3. Electrical noise affects the detector

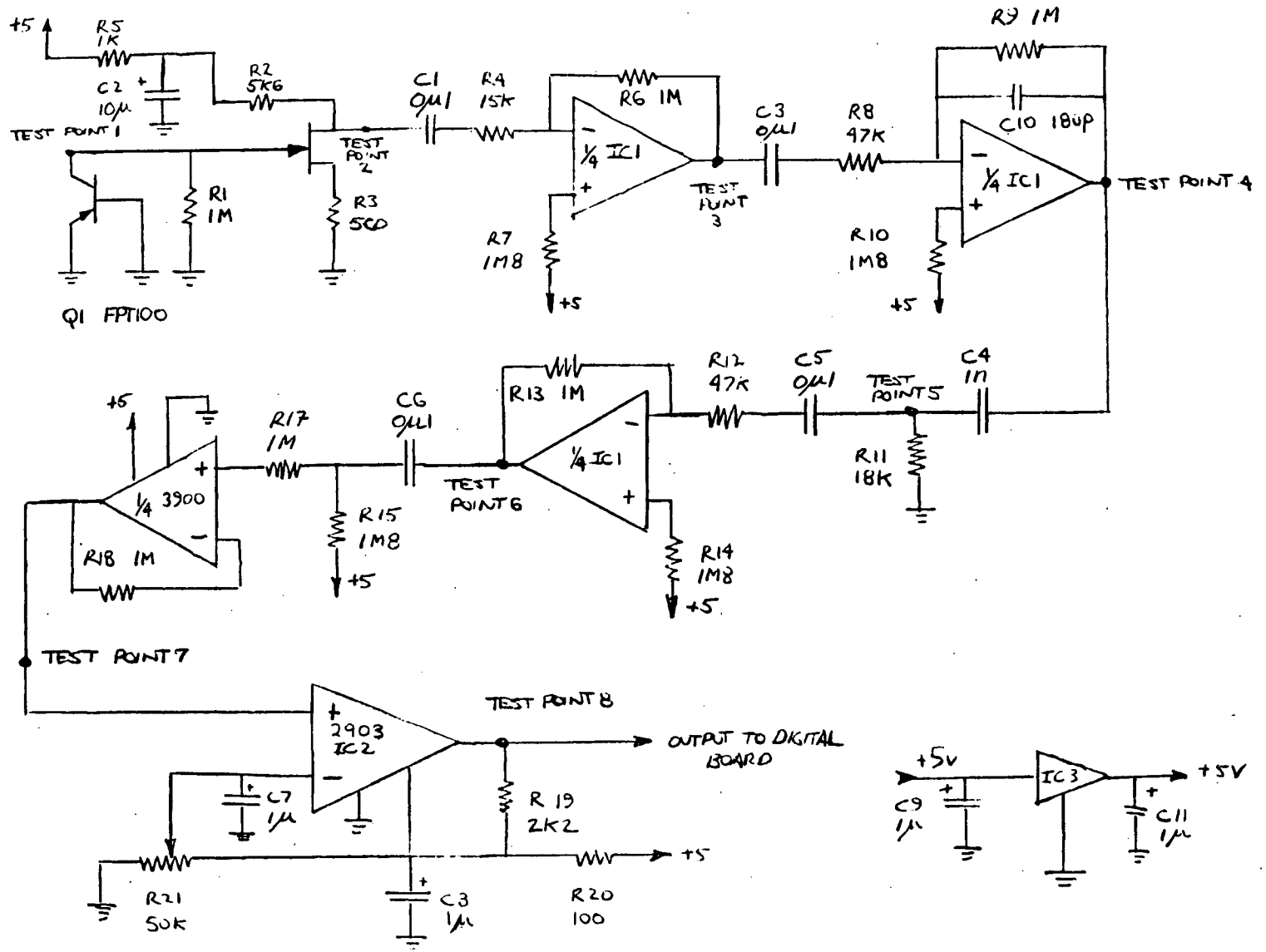

Figure 11 Circuit Diagram for Photodetector Amplifier and Pulse Shaper.

but can be virtually eliminated by shielding the electronics and by using a low pass filter.

In considering the meter as a whole the major considerations are the effects of nearby conducting objects (or people) and the separation between the sensor and the detector. Experiments[8] have revealed that when a person enters an electric field the field is distorted at distances up to 2 m away from the person. Thus in using the meter for making undisturbed measurements care should be taken in maintaining a reasonable distance (order of meters) from large conducting objects. On the other hand if one wishes to measure the enhanced field near a conducting object (say the head of a person) then the sensor can be brought very close. However, the sensor should be maintained about 10 mm away from pointed metallic objects. This is required because pointed objects have such a large enhancing effect that they can lead to corona discharge in the air and in the gas inside the sensor. The corona discharge produces light and invalidates the true reading of the meter. In all measurements the detector should be maintained at least 0.5m (this distance is derived experimentally) from the sensor in order that its metallic parts do not influence the reading. If a compact design of GEM is required in which the sensor and detector are one unit, then the meter has to be calibrated as one unit and can only be used reliably in uniform fields.

4.3 Summary

An electric field meter based on the breakdown of gas in an insulating vessel is constructed of three parts: the sensor, the fiber and the detector. The sensor produces light pulses whose number is proportional to the electric field. The fibre conveys these pulses to the detector where they are counted and displayed.

The specifications for the meter are summarized in Table 2. The entry for temperature is derived experimentally and further discussed in Section 5.

The last two sections have presented the physical model for the sensor and the design of the meter. These sections are partly based on a series of experiments performed during the development of GEM and its physical model. These experiments are the subject of Section 5.

Table 2

GEM Preliminary Specifications

Accuracy	better than 5%
Calibration	seldom required (every few months)
Size	
Sensor (including holder, spherical bulb)	45mm diameter x 55mm length
Fibre	2mm diameter x 2m* length
Detector	110 x 60 x 30mm
Power	9v rechargeable battery (10 hours operation)
Threshold	14 kV/m (can be reduced by increasing sensor dimensions)
Environmental effects	
Humidity	no effect
Above room temperature	no effect
Below room temperature	unknown

* variable

5.0 Experimental Results

5.1 Introduction

The purpose of this section is to describe in detail the experiments performed during the development of GEM and its physical model. Most experiments are performed in the laboratory where electric fields are generated between large parallel plates. Some experiments are performed just outside the laboratory in order to study environmental effects. Furthermore, some field tests both under typical transmission lines and in substations have been carried out.

Experiments outside and field tests are performed with a full prototype meter. However, in the laboratory it is more desirable to replace the detector with a more sensitive photomultiplier. The photomultiplier signal can be viewed directly on the oscilloscope (ie. the detector signal would have to be amplified and therefore distorted) and/or counted with a digital counter. Thus in the laboratory only the sensor (often without the holder, since the environment is controlled) and the fibre of the meter are used.

Four major series of experiments carried out in the laboratory and its immediate vicinity are described. The first series deals with the basic phenomena of pulse emission in uniform fields of fixed direciton. This set of experiments established the validity of the basic physical model (Sections 3.2 and 3.3). The second series of experiments deals with the sensor shape. This set of experiments provided the backing for extending the physical model to the case when the breakdown is guided by the vessel walls. The operation of a directionally sensitive sensor is

based on these experiments (see Section 3.4). The third set of experiments deals with the operation of spherical and cylindrical sensors in planar rotating fields. This set of experiments provides an understanding of what the sensor measures when exposed to environmental fields which are not perturbed by a conducting object (see Section 3.5 and 4.2). Finally, the last set of experiments deal with engineering considerations such as stability of calibration, accuracy, temperature and humidity effects and field perturbation (by the sensor). It should be noted that the details of the experimental results presented in a given section are for the specific sensor described in the section. However, most experiments have been performed with many different bulbs and similar results have been obtained.

In what follows the laboratory experimental set up is described in detail. Then the procedure and results for each set of experiments are presented. Finally, results from field tests are given.

5.2 Experimental Apparatus

5.2.1 Introduction

The experimental apparatus consists of two main parts: a device for generating electric fields and equipment for monitoring and studying the light pulses. There are two devices for producing electric fields. One generates uniform field in a fixed direction the other a planar rotating field of variable ellipticity. The device that generates uniform fields and the pulse monitoring equipment will be described first, followed by a description of the device for generating planar rotating fields.

5.2.2 Apparatus for Generating Uniform Fields in a Fixed Direction and Studying Pulse Emission.

The electric field is generated between the plates of a parallel plate capacitor, as shown in Figure 12. The plates consist of 600mm x 600mm x 3mm square sheets of polished aluminum with bevelled edges and rounded corners (radius $\sim$ 150mm) which serve to reduce corona at high field strengths. They are mounted horizontally on lucite sheets (thickness 10mm) which are quipped with hinged lucite doors for safety purposes. The upper plate is supported by three 25mm diameter threaded lucite rods which can be screwed into the upper lucite sheet and permit this plate to be aligned correctly with respect to the lower one. The plates are parallel to each other ($\pm$ 1mm) and the variable spacing is normally set at a distance of 150mm. The sensor is mounted on a lucite

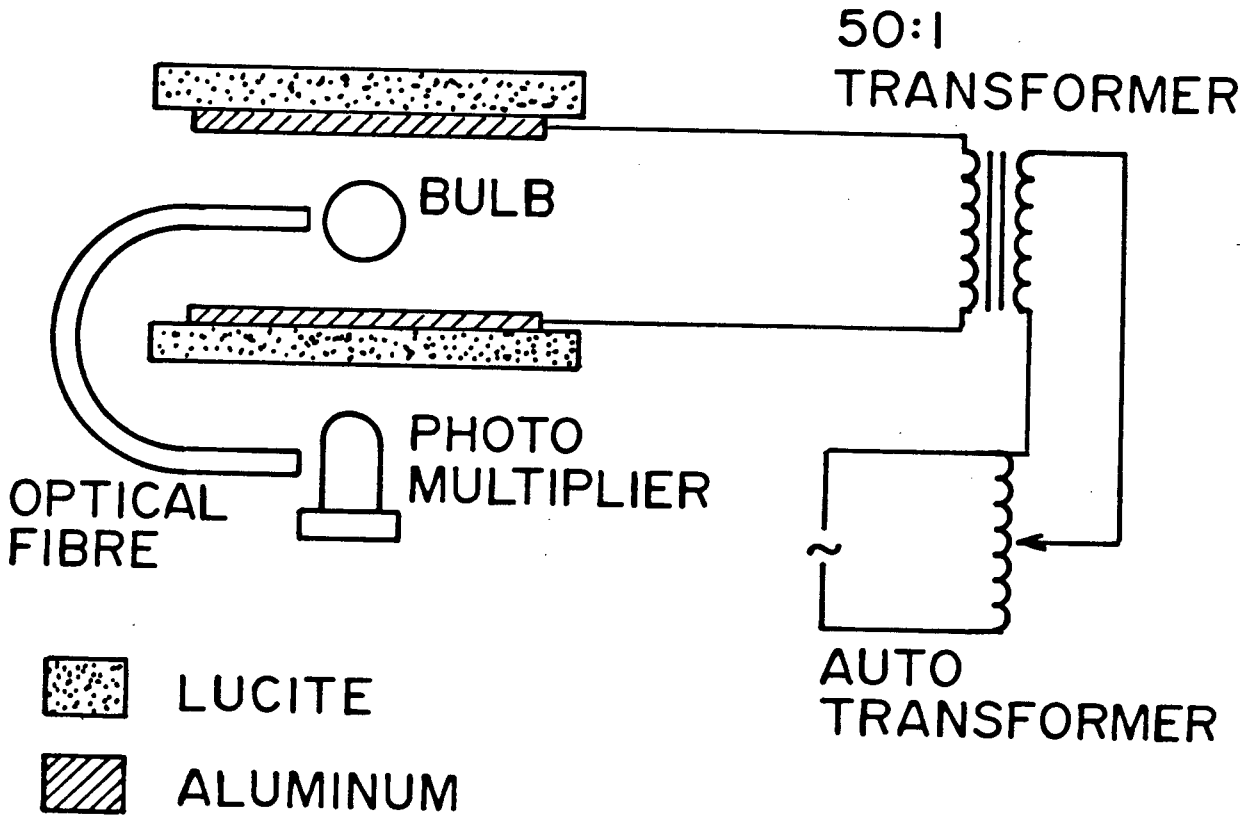

Figure 12 Experimental Set Up

bracket at the center of the field generated by the plates, so that it does not influence the charge distribution on the plates[21]. This location of the sensor also ensures that the applied field is spatially uniform.

The capacitor is normally powered by a 50:1 transformer fed by an autotransformer ('Variac') such that a maximum potential difference of 6kV (rms) occurs between the plates. This corresponds to a field strength of 40kV m^{-1} (rms) at a frequency of 60Hz. In some experiments a programmable power supply is used instead (Kepco, Model OPS 5000, gain 1000, maximum output 5kV). This facilitates studies of the effect of frequency and wave form shape on the sensor response. The frequency range employed extends from a few Hz up to 600 Hz. The voltage applied to the plates is measured directly with a high voltage potential divider.

The flashes of light emitted by the bulbs are conveyed to an RCA 931A photomultiplier through the vinyl clad glass fibre bundle (1.5m long, 2mm in diameter) obtained from Welch-Allyn Co. The photomultiplier is operated with its cathode at -1kV with respect to ground. The signals are recorded photographically using a storage oscilloscope (Tektronix Inc., Model 549 with a Model CA plug-in amplifier). The output from the oscilloscope amplifier (which contains a replica of the signal displayed on the oscilloscope) is fed to the counter (Advance Instruments, Model TC9A, 32 mHz). The counting interval is usually in the range of one to ten seconds.

All experiments (except for those involving the study of environmental effects) are carried out at 293 ± 4 Kelvin and less than 70% relative humidity.

5.2.3 Apparatus for Generating Planar Rotating Fields[22]

The 60 Hz planar rotating fields are produced by four vertical metal plates. The plates consist of 260mm x 760mm x 3mm sheets of polished aluminum with bevelled edges and rounded corners. They are mounted vertically on lucite sheets and form a square array when viewed from the top (see Figure 13). The sensor is mounted in the center of the device on a vertical hollow lucite rod. The optical fibre is mounted inside the lucite rod and emerges from the apparatus at the bottom (see Figure 13).

The four plate capacitor is powered by two parallel circuits each powered by a 50:1 transformer fed by a "Variac". The two transformers are driven by signals 180° out of phase. Each circuit consists of a bridge network which generates two voltages (V_1, V_2 and V_3, V_4) 90° out of phase with each other (see Figure 14). By connecting each of these voltages (V_1, V_2, V_3 and V_4) to adjacent plates of the capacitor an elliptically polarized field can be generated. The ellipticity of the field can be varied by changing the resistance values in the bridge network (see R_{21}, Figure 14). The magnitude of the field can be varied by changing V_o. The apparatus is capable of generating fields of up to 30 kV/m.

The flashes of light are conveyed to the same apparatus described previously. Figure 15 shows a picture of the apparatus.

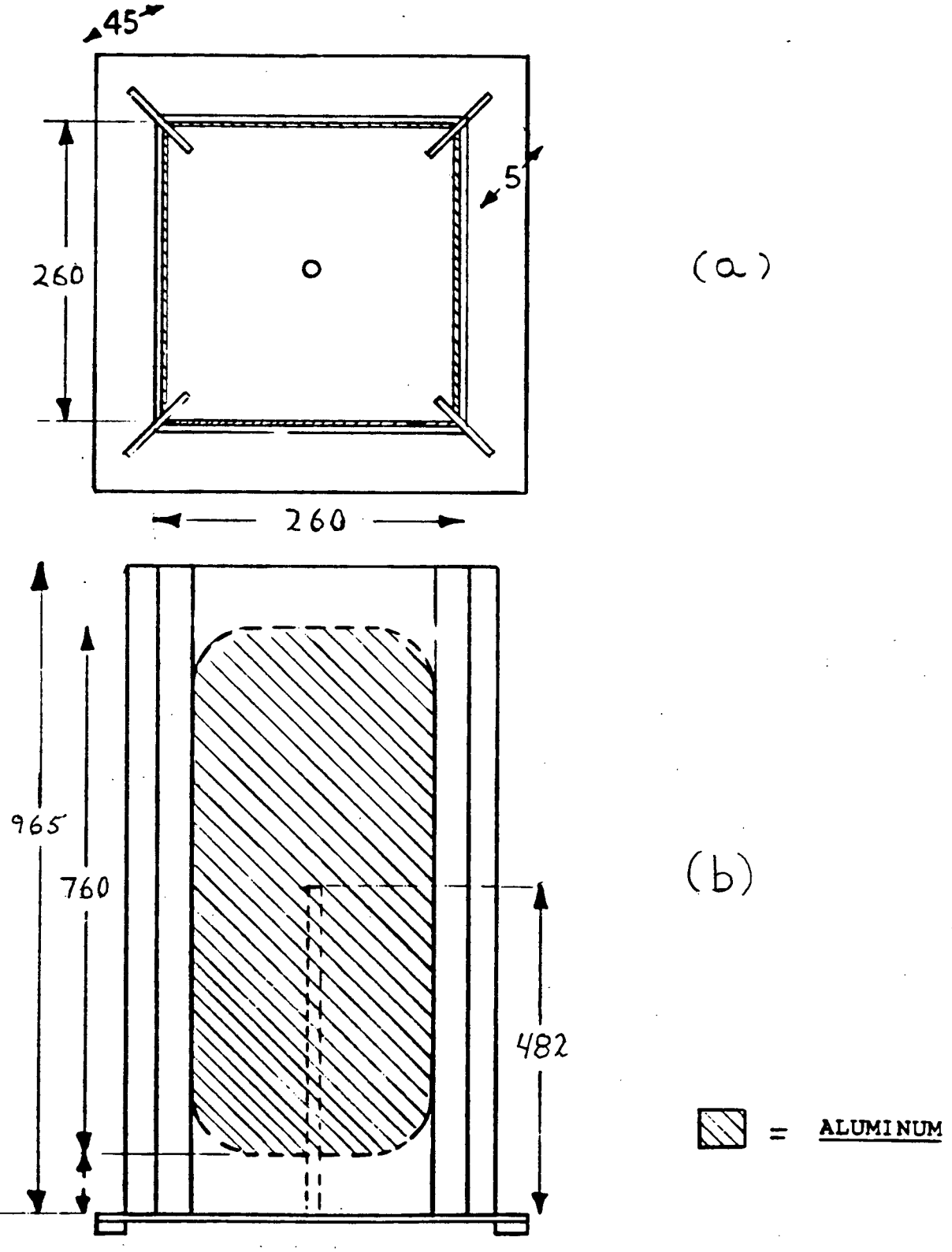

Figure 13 Apparatus for Producing Rotating Fields

(a) Horizontal section through centre

(b) side view

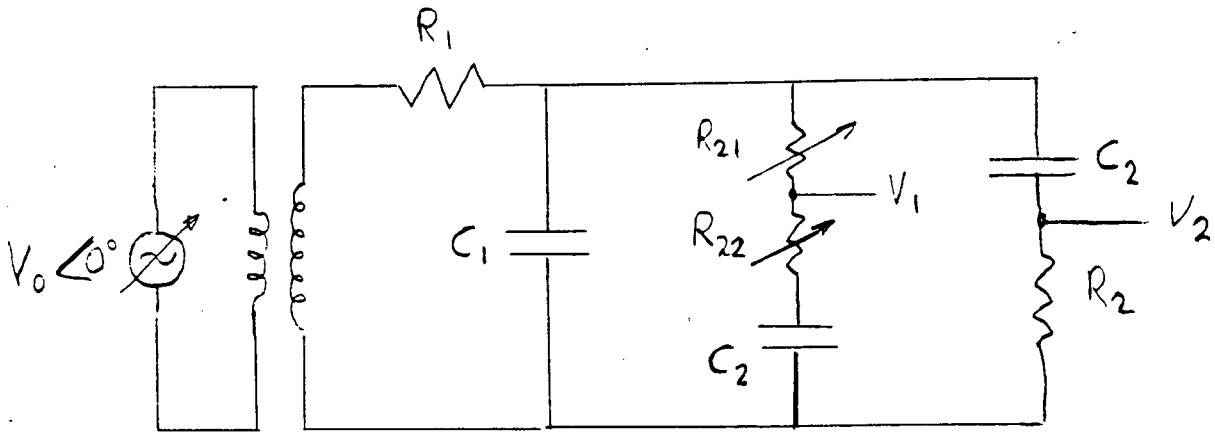

$R_1 = 0.3\ M\Omega$ $\quad R_{21} + R_{22} = R_2 = 2.5\ M\Omega$

$C_1 = 2700\ pF$ $\quad C_2 = 1000\ pF$

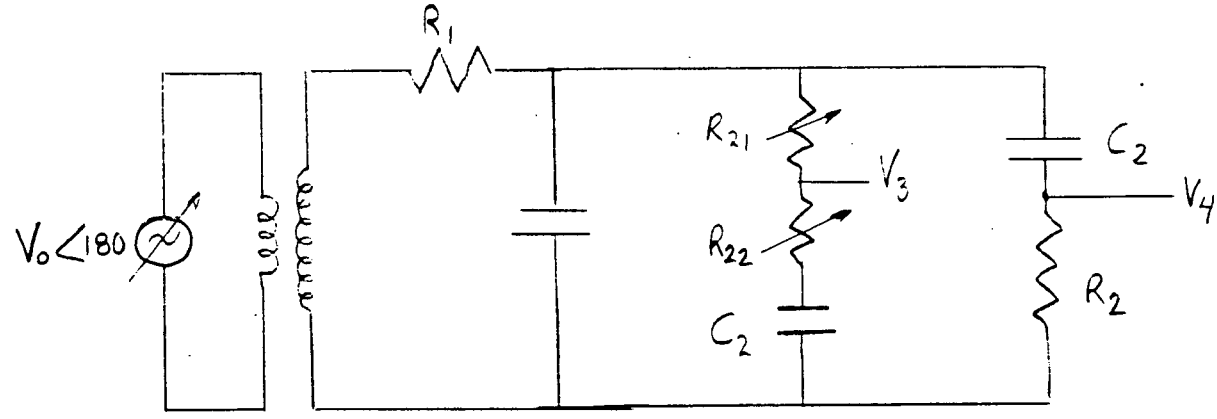

PHASOR DIAGRAM

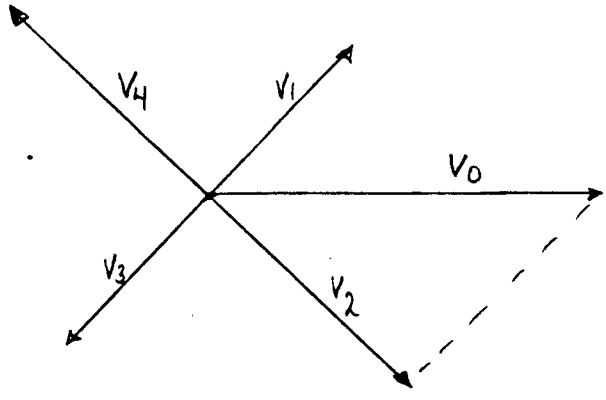

$$\frac{|V_1|}{|V_2|} = \frac{R_{21}}{R_2}$$

Figure 14 Electric Circuit for Generating Rotating Fields

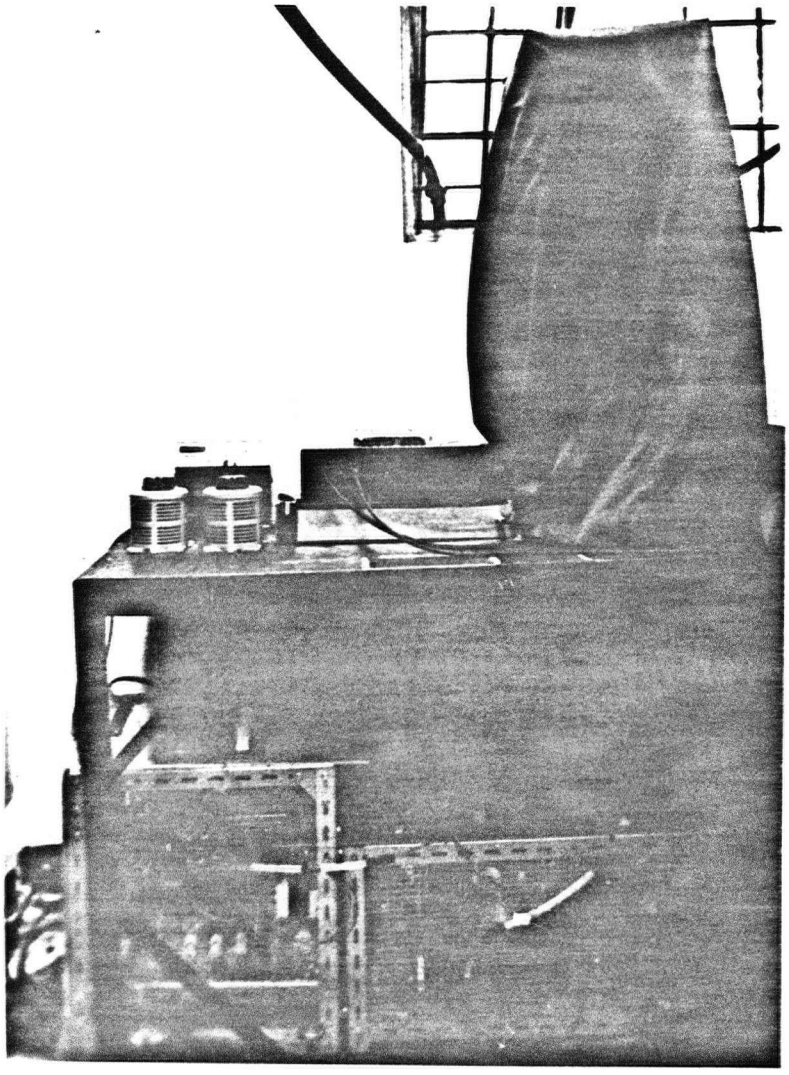

Figure 15 Photo showing plates for production of 60Hz rotating electric fields (right), 5 channel photomultiplier, variacs for driving the transformers (left), and electronics (bottom)

5.3 Study of the Basic Phenomenom

The experiments performed to investigate the basic phenomena are described in two sub sections. The first deals with all major features of the standard phenomena, the second deals with attempts to reduce the threshold by using different gas compositions.

5.3.1 Standard Phenomena

5.3.1.1 General Pulse Emission

This experiment is performed with a pyrex bulb of 25mm diameter filled with neon to a pressure of 10 Torr. The applied field is a 60Hz waveform whose magnitude is varied.

The relation between pulse emission and the phase of the applied field is observed by adding the measured voltage across the plates and the photo-multiplier output. The oscilloscope display of this signal shows the light pulses superposed on the applied field. A typical oscilloscope trace triggered on the applied field has been traced in Figure 16. The pulses of light appear on the rising and falling slopes of the sine wave. From many such pictures it is observed that the light pulses on a given slope of the applied field are spaced so that the change in the magnitude of the applied field is approximately constant. This change E_o in the applied field required to produce a new pulse is approximately the same on rising and falling slopes. However the change in field between the last pulse in a rising/falling slope and the first pulse of a falling/rising slope is usually slightly less than E_o. This

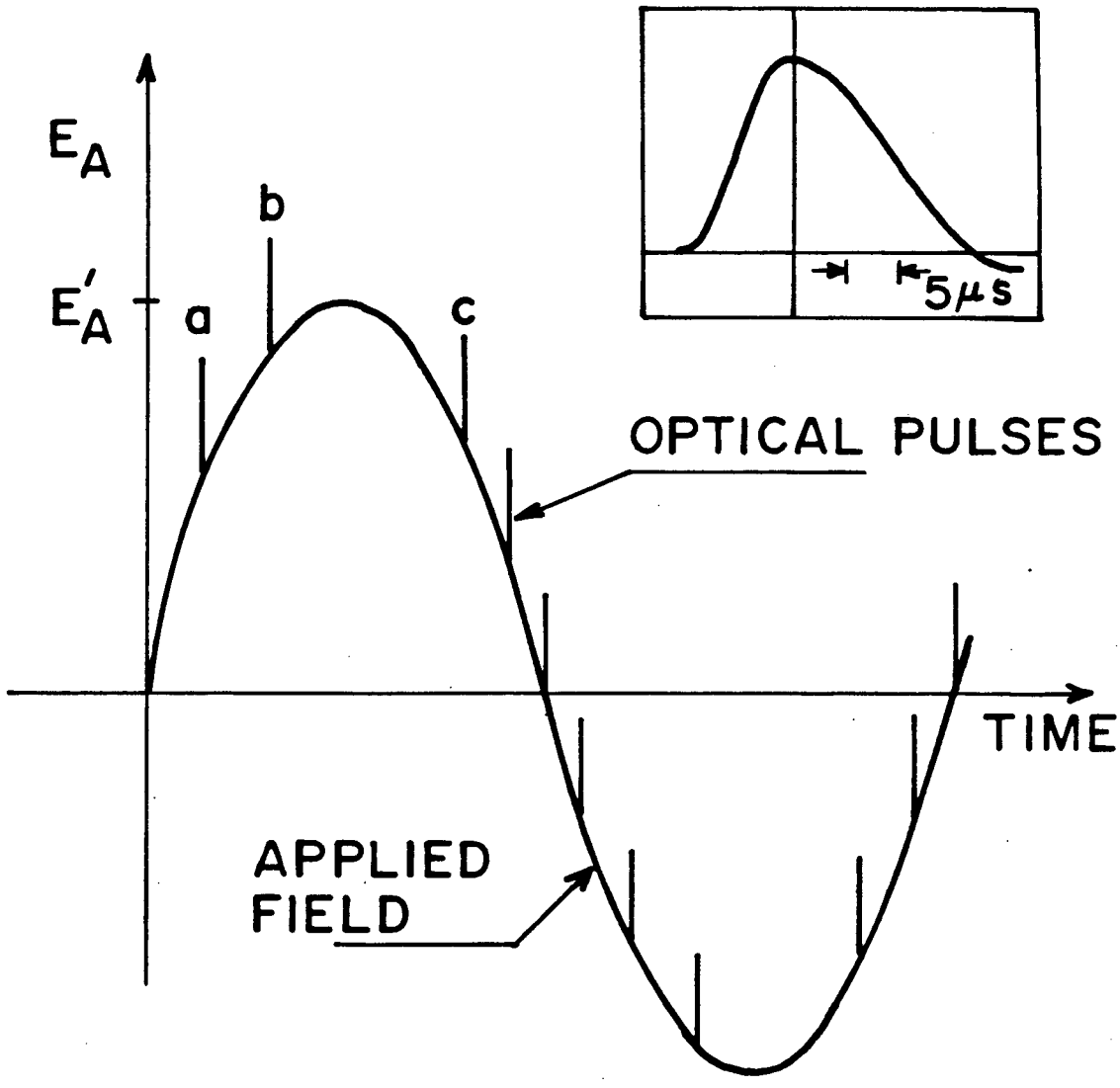

Figure 16 Optical pulses superposed on applied field wave form (E_A) for 25mm diameter neon-filled bulb at 10 Torr (strong breakdown case).

E'_A = field amplitude.

difference is consistant with the effect of finite conductivity which causes the field inside the bulb (E_T to be phase shifted with respect to the applied field (E_A) (see Section 3.3.5). In fact, if the graph of E_A versus time is displaced slightly to the left (becoming E_T versus time) pulses a and c (in Figure 16) will occur at idential field strength. When the peak to peak value, $2E_A'$, of the applied field is less than the threshold field, E_o, no light pulses are seen. As E_A' is increased above $E_o/2$ the bulb starts to emit pulses. For E_A' close to $E_o/2$ it can take a very long time for the first pulse to appear. For a field, E_A', higher than E_o the bulb "starts up" almost immediately. As the applied field is decreased pulses are observed until E_A' decreases below $E_o/2$. Thus there is a start up hysteresis. These results are consistent with the strong breakdown model.

5.3.1.2 Rate of Pulse Emission as a Function of Applied Field Magnitude

This experiment is performed with the same equipment as the previous one but the bulb pressure is also varied.

For fields above threshold and pressures higher than 10 Torr the situation is as depicted in Figure 16. The number of pulses emitted per cycle of the applied field depends on the integer number of times that E_o fits into $2E_A'$. An illustrative plot of this effect is obtained by measuring f_B, the number of pulses per second (averaged over one second) versus E_A'. Such a plot consists of steps of size $E_o/2$ in applied field and of size 120 Hz in f_B (ie. twice f_A, the frequency of E_A'). Figure 17 shows such a plot. The same effect is observed for higher bulb pressures, except that the steps become sharper. However for the lower

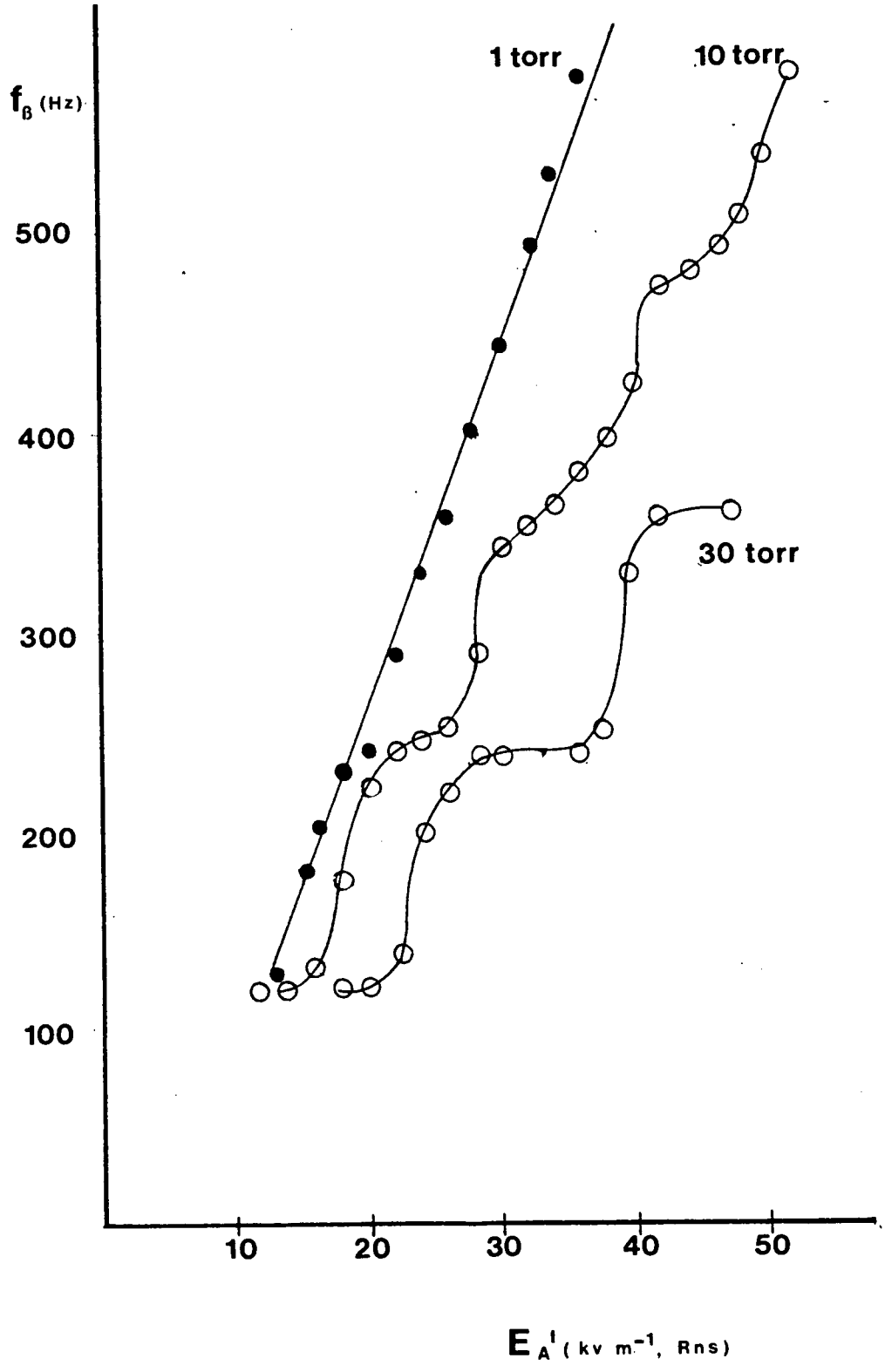

Figure 17 Pulse emission frequency (f_B) as a function of applied field (E_A') for different bulb pressures.

Bulb diameter was 25mm.

pressures the steps are gradually smeared out until at 1 Torr the relationship between pulse frequency and applied field is linear (see Figure 18). Another effect of low pressures is that the threshold is not sharply defined at $E_o/2$ and pulses are emitted for $E_A < E_o/2$. However results are not reliable in this regime.

For bulbs filled to pressures of 10 Torr or greater, the change in applied field (ΔE_A) between pulses in effectively constant. However at pressures less that 10 Torr ΔE_A begins to fluctuate. It commonly fluctuates by a factor of two at pressures less than 1 Torr for a constant amplitude (E_A') of the applied field. Figure 4 shows a typical waveform for a low pressure bulb, obtained in the same way as the one shown in Figure 16. In comparison, at pressures exceeding 10 Torr ΔE_A fluctuates by less than 15%. Clearly, it is the variations in ΔE_A that smear out the steps in Figure 17. It is also clear from Figure 4 that ΔE_A depend on the pulse height.

The pulse height is a measure of the amount of light emitted or the strength of the breakdown avalanche. Pulse height varies at all pressures. The variation at a given pressure depends on the different bulbs. At high pressures the variation is much less than at low pressures. At lower pressures, the field increment between successive pulses increases with the height of the first pulse as can be seen in Figure 4.

These results indicate that weak breakdown occurs at the lower pressures. At these pressures it is harder to reset E_I completely to 0. It is in this regime that one needs to operate GEM if a linear relation between E field and count rate is desired.

Finally, it must be observed that pulse shape is remarkably constant (for an example see insert in Figure 16) for the pressures tested from 1 to 30 Torr. Furthermore the total duration of the pulse is independant of its height. The area under the pulse profile (ie. the amount of light emitted) is therefore proportional to its height as has been assumed above.

5.3.1.3 Determination of E_o

This experiment is performed with a series of bulbs whose diameter ranges from 12.5mm to 38.1mm and whose pressure ranges from 0.66 Torr to 30 Torr. The applied voltage is a 60Hz waveform whose magnitude is varied.

We have seen that E_o is a well defined quantity for high pressures. It is the change in the applied field necessary to obtain a new pulse (averaged over falling and rising slopes). At low pressures the change in applied field required to obtain a new pulse fluctuates widely. However defining E_o as the change in the applied field required to change the pulse frequency by 240Hz allows comparison of low pressure and high pressure results. Also $E_A' = E_o/2$ is defined as the threshold for bulb operation (assuming the bulb is started and the voltage lowered until 120 pulses/sec are observed). At high pressures this is a true threshold, but at low pressures, pulses are observed with $E_A' < E_o/2$. However, reliable results are only obtained for count rates greater than 120Hz.

The pulse rate was plotted against the applied field magnitude for a series of 25mm diameter bulbs filled with neon at pressures of 30, 10, 5

and 1 Torr pressure. Results indicated that the 10, 5 and 1 Torr bulbs had an E_o of around 42±3 kV/m. This is within the reproducibility of the bulb characteristics. However the 30 Torr bulb had an E_o of 59kV/m.

This result indicated that the optimal threshold is relatively independent of pressure for pressures below 10 Torr. The results are consistent with the Paschen's law with a broad minimum in, $\emptyset$, (see Equation 1). The validity of this law was also checked for three bulbs having a pd of 25mm Torr (diameters 12.5mm, 25mm and 38mm). The results indicated the threshold field varies inversely with bulb diameter for fixed pd. $E_o d$ was found to be about 1000 volts (see Figure 18). By setting pd near the Paschen minimum, the threshold, $E_o/2$, can be reduced by increasing the bulb diameter since $E_o = 1000/d$. Fortunately the Paschen minimum is sufficiently broad to encompass a pressure of 1 Torr with bulbs of convenient size, such that pulse frequency is proportional to the applied field.

The set of experiments described so far establish the basic physical model for uniform fields of fixed direction and for bulbs whose walls do not interact with the discharge. However, another set of experiments in which the wave profile and frequency of the applied field is varied was performed to further check the basic assumption of constant E_o and the effect of finite conductivity.

5.3.1.4 Pulse Emission: Dependence on the Applied Waveform

This investigation is performed with a pyrex bulb of 25mm diameter filled with neon to a pressure of 10 Torr. The applied field is a programmable waveform whose frequency can be varied from 1Hz to 600Hz.

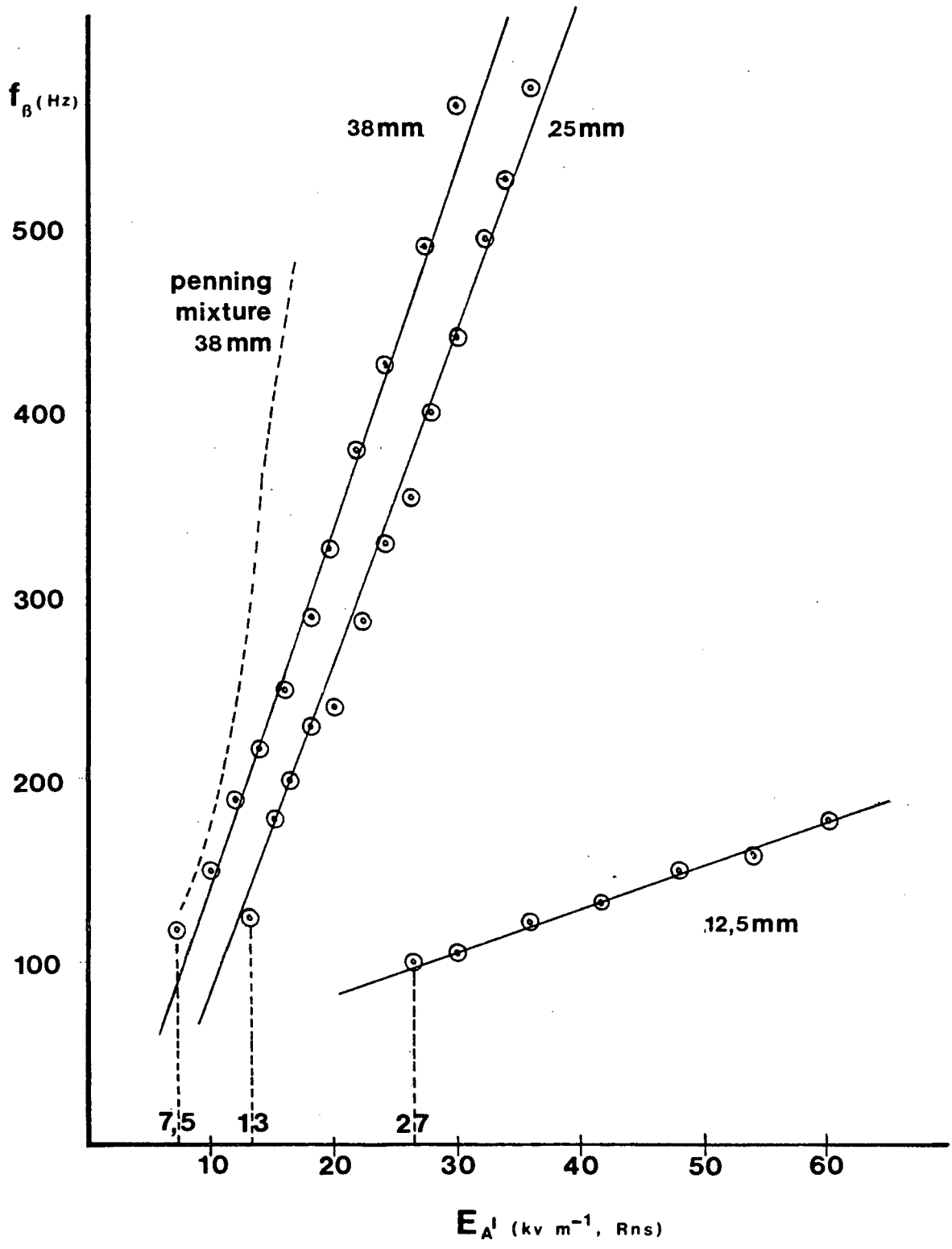

Figure 18 Pulse emission frequency as a function of applied field for different bulb diameters.

Bulb pd was 25mm Torr

Different Frequencies

Varying the frequency of the applied field does not change the phenomenon. The number of pulses emitted per cycle depends only on the field magnitude (1Hz to 600Hz) not on the rate of change of the field.

Pictures of the pulses superposed on the applied field for 6Hz, 60Hz and 600Hz frequencies are very similar provided the appropriate time scales (50 ms/d, 5ms/d, 0.5ms/d) are chosen. However at 600Hz it is common to see reliable operations for $2E_A' = E_o$ with one pulse on the maximum and one on the minimum of the sine wave. At this frequency the screening effects due to the bulb conductivity are negligible.

Operation above 600Hz has not been investigated due to the lack of equipment for generating the fields. However, it is clear that the effect will be similar until the frequency approaches the inverse of the pulse width (kHz region). For frequencies below 1Hz the bulb operation is unreliable: pulse emission is sporadic even for fields high above threshold. For time independent fields, pulses are observed when the field is turned off or on. Maintaining a very high static field will, at times (especially for bulbs at low pressure), cause pulses to be emitted separated by a few seconds. However this is only observed for very low gas pressures (0.65 Torr).

Different Waveforms

The above experiments can be repeated with various waveform shapes. Of special interest is a square wave since it contains large time

intervals of constant field, where pulses should not appear. Figure 19 shows such a wave. Pulses are observed only when the field changes. Triangular waves for which each slope is constant are useful in confirming the pulse emission at constant E_o by checking for emission at constant time intervals during each rising/falling slope of the field.

These experiments confirm the validity of equation 2 for a broad range of frequency ($1 < f_A < 600$Hz). Furthermore, they confirm that waveform shape is not important to the phenomena, only peak to peak field magnitude matters.

5.3.2 Possible Mechanisms to Reduce the Threshold

The most promising mechanism to reduce the threshold is the Penning effect. This experiment is performed with a 25mm pyrex bulb filled with a Penning mixture of Ne and 0.3% Ar to a pressure of 18 Torr. The applied field is a 60Hz wave form whose amplitude is varied.

A typical oscilloscope trace for this Penning bulb is shown in Figure 20. As can be seen the effect is different. Instead of the uniform height pulses equally spaced, there is one large pulse followed by a series of small pulses getting progressively closer. The threshold for the first pulse is very close (ie. within 1kV/m) to the threshold for non Penning mixtures. However as can be deduced from Figure 21 the threshold for subsequent pulses is much lower (2 to 10 times). Thus a graph of the frequency (f_B) of optical pulses versus applied field is similar to normal bulbs but has a much larger slope as shown by the dotted line in Figure 18.

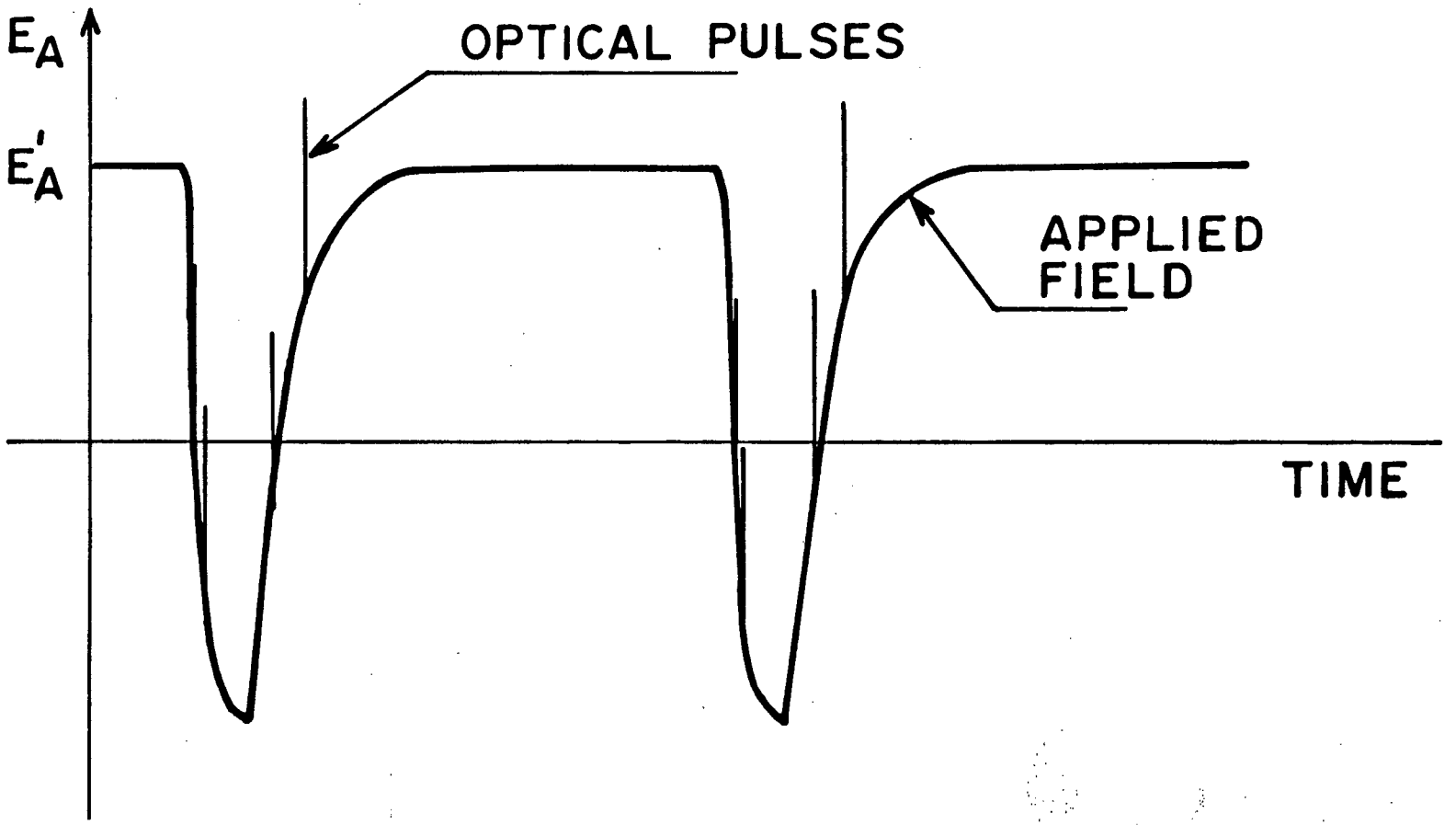

Figure 19 Optical pulse superposed on applied waveform (E_A)

- pulses occur only where E_A varies in time.

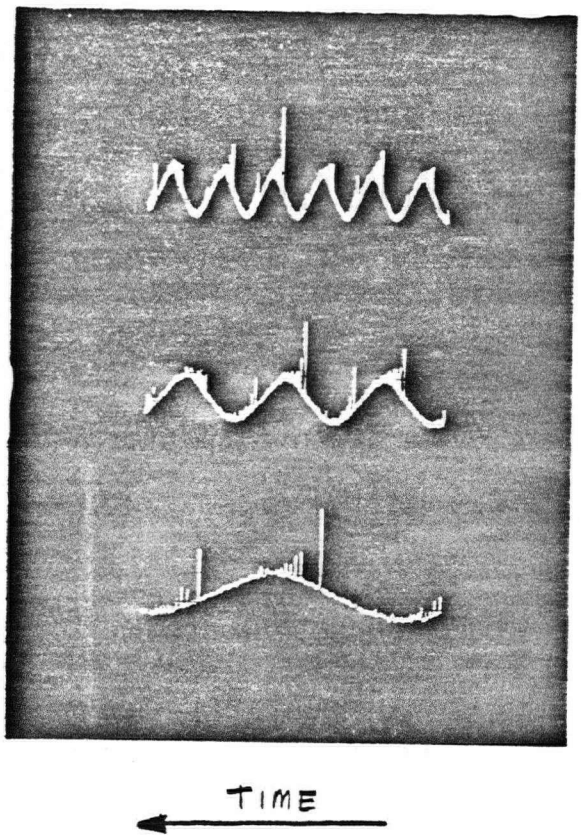

Figure 20 Optical pulses superposed on the applied wave form E_A for a Penning mixture bulb (time runs left)

Similar results are obtained with other Penning mixtures. Clearly the expected Penning mechanism works only for the pulses following the first one and is therefore not useful in reducing the threshold of the sensor.

Another alternative to reduce the threshold is the addition of tritium to a gas.

Since impurities affect breakdown irrespective of whether they are radioactive or not experiments were carried out to determine what effects H_2 would have on the breakdown characteristics.

It was found that even very small percentages of H_2 produced bulb with clearly defined steps which are undesirable. Thus the best gases for bulb design are the inert gases (Ne and Ar).

5.4 Sensor Shape Investigations

The main thrust of these experiments is to understand the operation of a cylindrical tube placed at an arbitrary angle to a uniform electric field of fixed direction. However, a very simple experiment to show the isotropic response of a spherical bulb is described first.

5.4.1 Spherical Bulb

This experiment is performed with a typical spherical bulb (38mm diameter 0.66 Torr neon). The applied field is a 60Hz waveform whose magnitude is varied.

The bulb is first placed with its nipple (see Figure 8) horizontal (ie. parallel to an equipotential surface) and the threshold field is measured for different rotations of the bulb about a vertical line (perpendicular to the capacitor plates). The variation in threshold observed is less that 1%. Thus the response is isotropic. Next the bulb is rotated about a horizontal line with the diameter through the nipple perpendicular to the line. The threshold increases as the nipple deviates from pointing horizontally to pointing vertically. The change observed for this bulb was 19%. This result is not inconsistant with the extra length provided by the nipple.

Clearly the ideal spherical bulb is isotropic, however the isotropy of a real bulb depends on how well it is sealed off after filling.

5.4.2 Cylindrical Tubes

This experiment is performed with two cylindrical gas filled tubes. The fat tube is 12.5mm (diameter, D) by 55mm (length, L) and is filled to, 0.5 Torr Ar (this is within the Paschen minimum for both dimensions). The thin tube is 6mm (D) by 55mm (L) and is also filled to 0.5 Torr of Ar.

The tube under investigation is attached at its mid point to a horizontal insulating rod made of lucite. The rod, which is 75mm above the lower plate (see Figure 12), rotates the tube in a vertical plane. The angle, $\emptyset$, between the tube axis and the vertical (ie. the direction of E_A) can be set to an accuracy of $\pm 1°$ by means of the protractor fitted to the rod.

To measure f_B, light has to be collected from both sides of the tube (Figure 5 AD and BC). The fibre axis therefore is normally set along the tube radius in the plane of Figure 5. The light emission was also observed by setting the end of the fibre at various points along AD or BC, with the fibre-axis perpendicular to the plane of Figure 5. The light emission was also observed by setting the end of the fibre at various points along AD or BC, with the fibre-axis perpendicular to the plane of Figure 5. These studies showed that the internal field (E_I) is directed away from the side of the tube from which the light is emitted. Time-integrated photographs also show that the breakdown discharge takes the form of the shaded region in Figure 5 when E_I is along the $+\underline{z}$ direction. When E_I is along the $-\underline{z}$ direction the breakdown discharge goes from C to D to A and is thickest at A. For the sake of clarity this portion of the discharge is omitted from Figure 5 but can be seen in the

photograph (Figure 21). The observations are consistent with the idea that the breakdown discharge is maintained by electrons accelerated by the internal field E_I and is guided by the tube walls.

The tubes operate reliably if $f_B \geq 120Hz$. Threshold conditions are therefore defined to be those at which $f_B = 120Hz$. The threshold field for breakdown was measured for the wide tube (D = 12.5mm) with the tube axis along the applied field, or perpendicular to it. It was found that

$$E_{OP}/E_{ON} = 12.4kVm^{-1}/50kVm^{-1} = D/L$$

where E_{OP} and E_{ON} are the respective threshold fields for the tube axis parallel or normal to the applied field. It therefore follows from the above equation that

$$V(0) = V(90)$$

where $V(0) = E_{OP}L$ is the potential difference at threshold between the tube ends with $\theta = 0°$, and $V(90) = E_{ON}D$ is the potential difference at threshold across the vertical diameter with $\theta = 90°$. This equation is consistent with the notion that the breakdown conditions satisfy the Paschen rule (Equation 1) with $\emptyset$ near its broad minimum. The results also show that the fields are not significantly attenuated by the flow of conduction currents in the glass (ie. E_N has the same strength both outside and inside the tube).

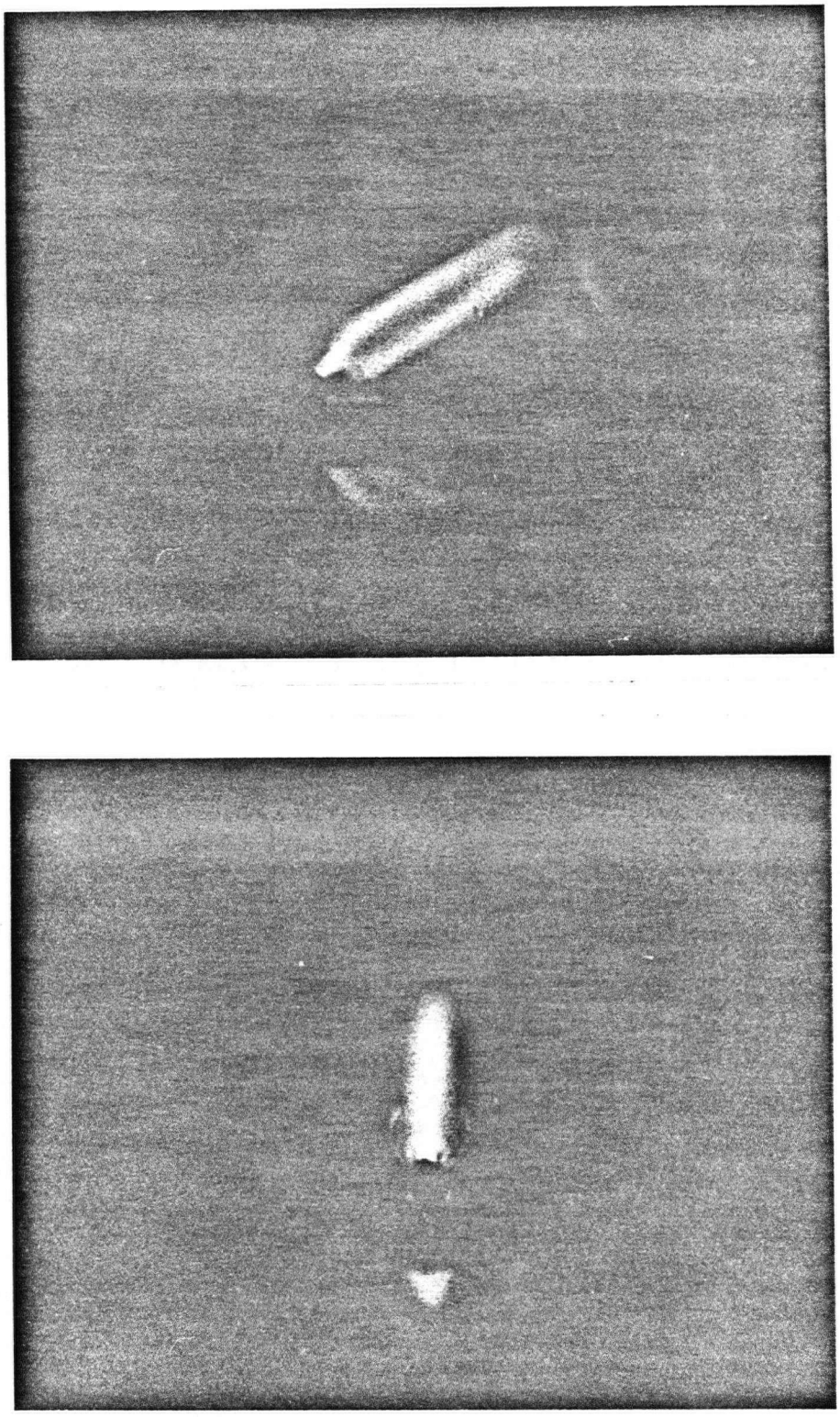

Figure 21 Time integrated photographs showing the breakdown discharge in cylindrical tubes. The electric field is vertical.

To minimize the effect of the "free travel" part of the discharge, (AB and CD in Figure 5) further studies were done with the narrow tube (D = 6mm, L = 55mm). With the tube vertical ($\theta = 0$), the frequency of breakdown (f_B) was measured as a function of the potential difference $V_A = E'_A L$ along the tube. f_B satisfies the calibration equation (see Figure 22, curve a)

$$f_B = 380(V_A - 0.54) \qquad \text{for } V_A \geq 0.85\text{kV}$$

$$= 0 \qquad\qquad V_A < 0.85\text{kV}$$

where V_A is in kV and f_B in Hz. To maximize the frequency of breakdown $f_B(\theta)$, in a tube inclined at an angle, θ, to the applied field, the amplitude of the field in the gap was maintained at its largest value of $E'_{Am}=53\text{kVm}^{-1}$. $f_B(\theta)$ was then measured for $0 < \theta < 75°$. This curve is shown in Figure 22 (curve b). If the breakdown discharge does not lose significant amounts of energy in its interaction with the wall, then the frequency of breakdown should depend only on the potential difference between the two ends of the tube, irrespective of the angle θ.

To check this hypothesis we define E''_A as the field amplitude which produces a particular value of the breakdown frequency, f'_B, with the tube mounted vertically. The same breakdown frequency will therefore occur when $\theta = \theta'$ provided that the potential difference acrossthe tube remains unchanged, ie. that

$$E''_A L = E'_{Am} L \cos\theta' \qquad (6)$$

Thus a plot of E''_A/E'_{Am} against $\cos\theta$ should be a straight line of unit

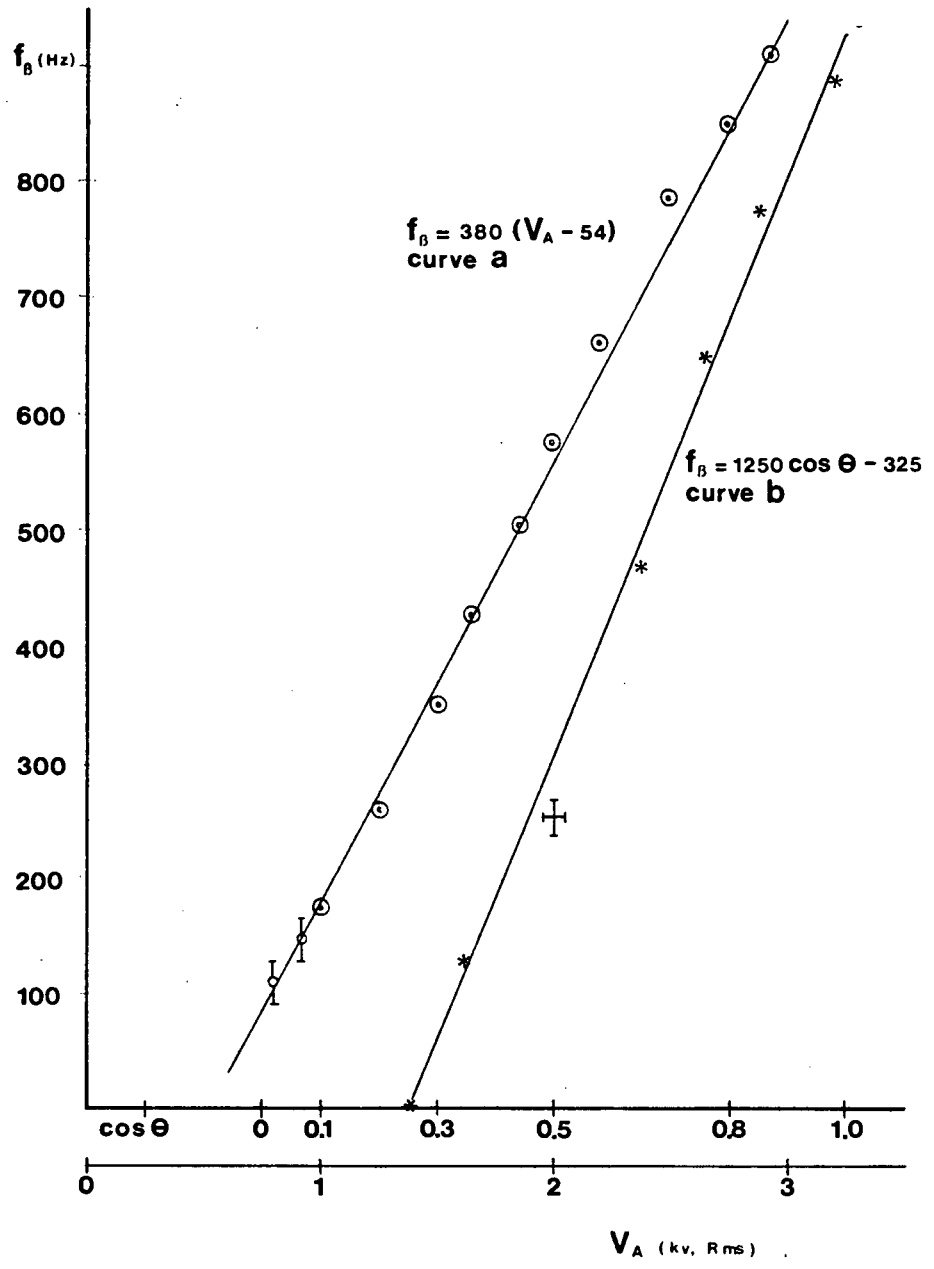

Figure 22 Frequency of breakdown as a function of potential difference along the tube (V_A) (curve a) and as a function of orientation angle (cos θ) for fixed E_A^1 = 53kVm^{-1}(curve b). Bulb is 55mm x 6mm and filled with 0.5 Torr Ar.

slope, passing through the origin. The above discussion requires that the potential difference across the tube exceeds the threshold value (0.85kV in our case), so that Equation 6 applies provided cosθ 0.29.

It should be noted that Equation 6 is independent of the specific form of the calibration curve (Figure 21) provided that f_B is a single-valued function of V_A.

The plot of E''_A/E'_{Am} against cos θ' can be obtained graphically from Figure 22 as follows: select any count rate (say 400), cosθ' is obtained from curve b (0.58) and E''_AL is obtained from curve a (1.59kV). E''_A/E'_{Am} is obtained by dividing E''_AL by 2.92kV (ie. 53kV/m x 0.055m).

Figure 23 shows a plot of E''_A/E'_{Am} versus cosθ. The fact that it is an excellent straight line indicates that Equation 6 is valid.

The above results show that the frequency of breakdown in electrodeless tubes, immersed in low frequency fields, is governed by the potential difference between the ends of the tube, provided the discharge is guided by the tube walls. They also show that energy losses in the wall-discharge interaction are not significant. If they were, then V(θ) would have to be larger than the value predicted by the model presented above. Finally the results demonstrate that a narrow, cylindrical, gas-filled, insulating tube can be used to measure the component of a low frequency field along the tube-axis.

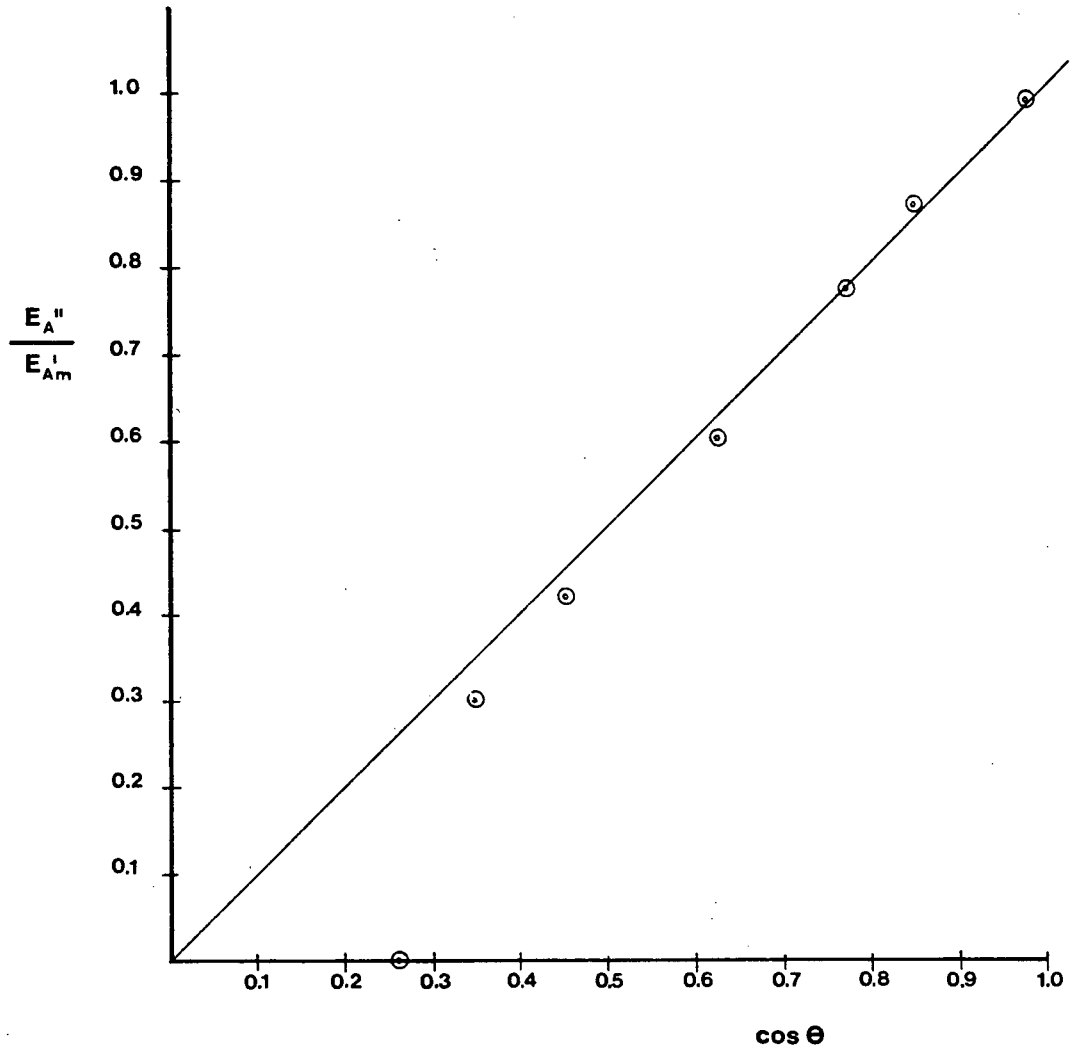

Figure 23 Normalized response of cylindrical tube as a function of the angle between the tube axis and the field direction.

5.5 Investigations of Planar Rotating Fields

The main thrust of these experiements is to understand the operation of spherical bulbs in planar rotating fields. However, a very simple experiment is described first to show that a cylindrical bulb responds to the component of the electric field along the bulb axis (see Section 3.5.2.1).

These experiments are performed with the apparatus described in Section 5.3.2.

5.5.1 Cylindrical Tube

This experiment is performed with the thin cylindrical tube (Section 5.4.2).

A circularly polarized field rotating in a horizontal plane at 60Hz is generated by the equipment described in Section 5.2.3. The cylindrical tube is placed in various directions in the plane of the field. The measurement (f_B) remains constant irrespective of tube orientation and is equivalent to the measurement obtained when the tube is aligned with a uniform field in a fixed direction of the same magnitude.

5.5.2 Spherical Bulbs

This experiment is performed with a 38mm, 1.3 Torr Ar lead glass bulb whose calibration curve has very distinct steps in a uniform field of fixed direction (see Figure 24)

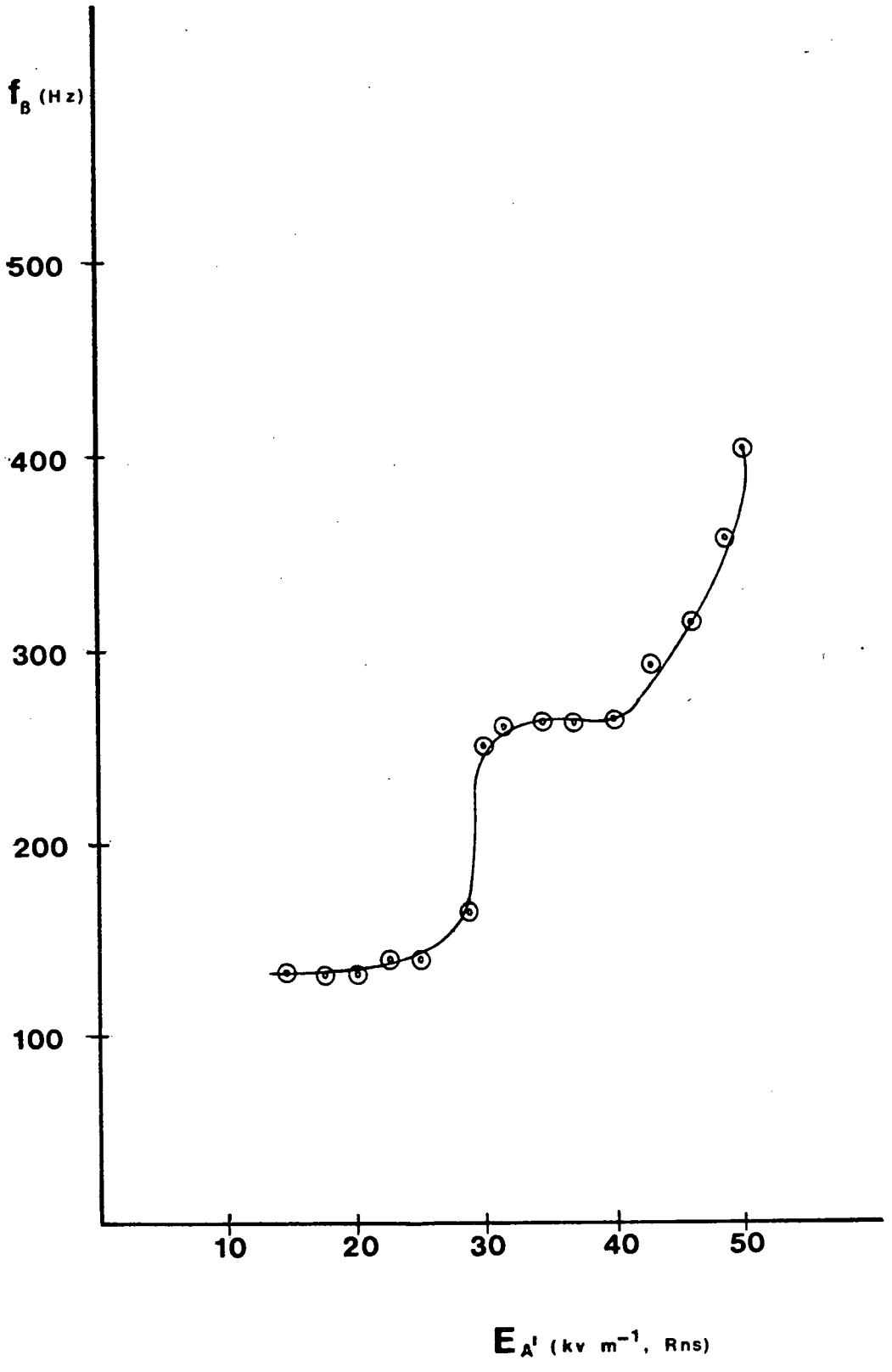

Figure 24 Pulse emission frequency as a function of applied field. 38mm, 1.5 Torr Ar, lead glass spherical bulb.

5.5.2.1 General Pulse Emission in Circularly Polarized Fields

The pulse emission observed is similar to that observed in fields of fixed direction, except for one major difference. The pulses are equally spaced in time and do not have any relation to the phase of the applied field. This observation is consistant with the model that a pulse occurs every time E_A' rotates through a fixed angle.

5.5.2.2 Rate of Pulse Emission as a Function of Field Magnitude and Shape

Figure 25 shows a plot of f_B versus the applied electric field for a circularly polarized field and a linearly polarized field (which is generated by grounding the plates that would normally be connected to V_1, and V_3 in Figure 14). As expected, the steps observed in the linear field disappear. The enhancement factor as defined in Section 3.5.2.2 is 1.67. It is obtained by taking the ratio of the slope of a line constructed from the calibration curve for circularly polarized field to one construced from the calibration curve for a linearly polarized field. For the circularly polarized field the line is the calibration curve itself. For the linearly polarized field it is the line drawn through the top of the step on the calibration curve. The observed enhancement is close to the theoretical value ($\pi/2$) expected for $E_A'/E_o > 2$. However the enhancement factor is observed for all values of E_A' above threshold. Furthermore, the threshold field is slightly lower in a circularly polarized field. This descrepancy between experiment and theory at the lower fields is probably due to the assumption that E_B is uniform. At high fields θ is small and $\underline{E}_A$ and $\underline{E}_B$ are approximately antiparallel

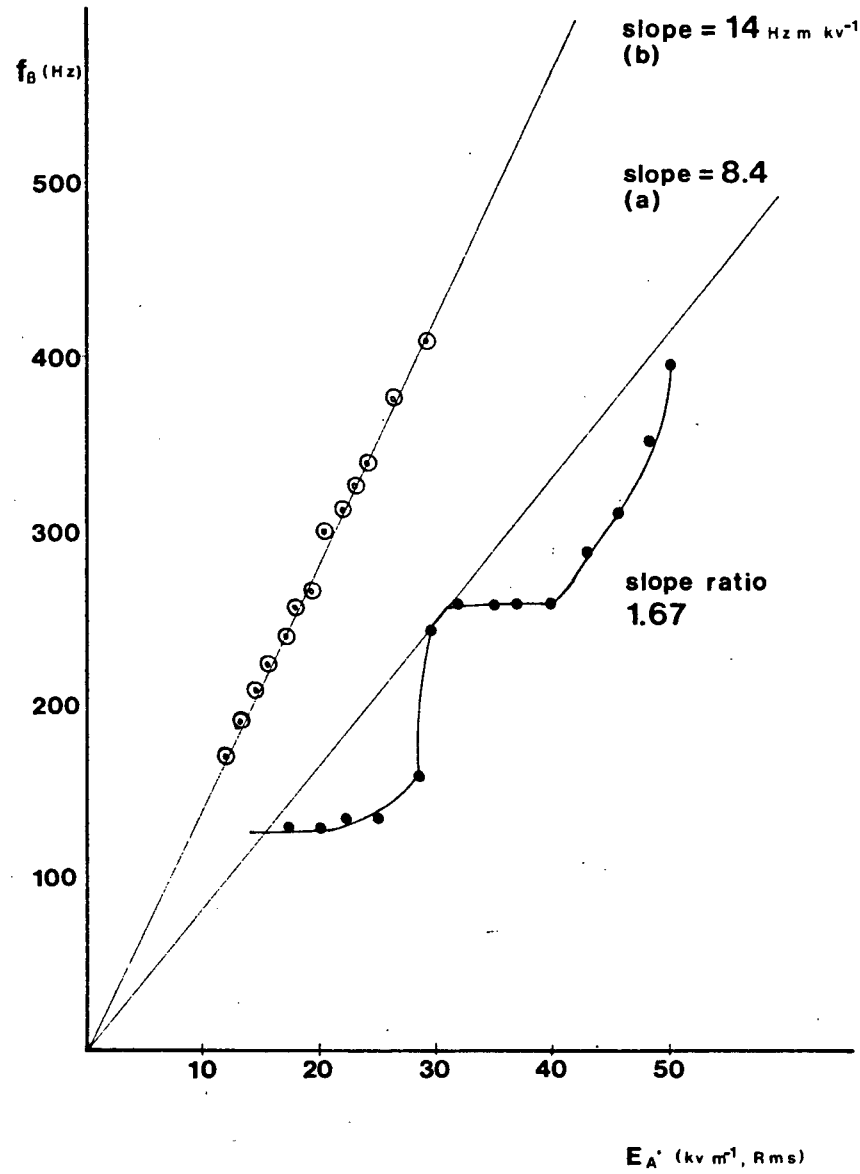

Figure 25 Pulse emission frequency as a function of applied field (a) linear field (b) circularly polarized field. 38mm, 1.5 Torr Ar, lead glass bulb.

(± a few degrees). For this situation the non uniformity of E_B should have little effect. However as θ becomes larger than 90° (say 120°) non-uniformities in E_B can lead to breakdown paths which are not straight and which may be more favourable than a path at θ = 180°. Since there are 180 pulses/sec at threshold θ must be 120 which is consistent with the above explanation.

The same experiment is repeated with planar rotating fields of different aspect ratios or ratio of semimajor axis field to semiminor axis field. These fields are generated by varying the ratio of R_{21} to R_2 in the electric circuit shown in Figure 14. Figure 26 is a plot of the results. Again the steps disappear (progressively earlier for more rounded ellipses) and the high field enhancement is very close to the theory (the ellipse circumference divided by 4 E_A'*). However, the steps disappear earlier than expected from a theory with uniform E_B (see Appendix II). For example, for an ellipse of aspect ratio 1:1/2 (ie. of semimajor axis to semiminor axis ratio of 2), the steps should disappear near twice the threshold (around 24kVm^{-1}) but they disappear almost at threshold (ie. at 14kVm^{-1}). This effect is similar to the enhancement observed at threshold in the circularly polarized field and is probably also due to the effect of non uniform E_B near threshold.

These results confirm the basic theory of operation of a spherical bulb in planar rotating fields well above threshold. They also indicate that for fields near threshold the theory is not as accurate, an observation which is consistent with possible effects due to a spatially non uniform E_B.

* recall that E_A' represents the semimajor axis field of the elliptical field.

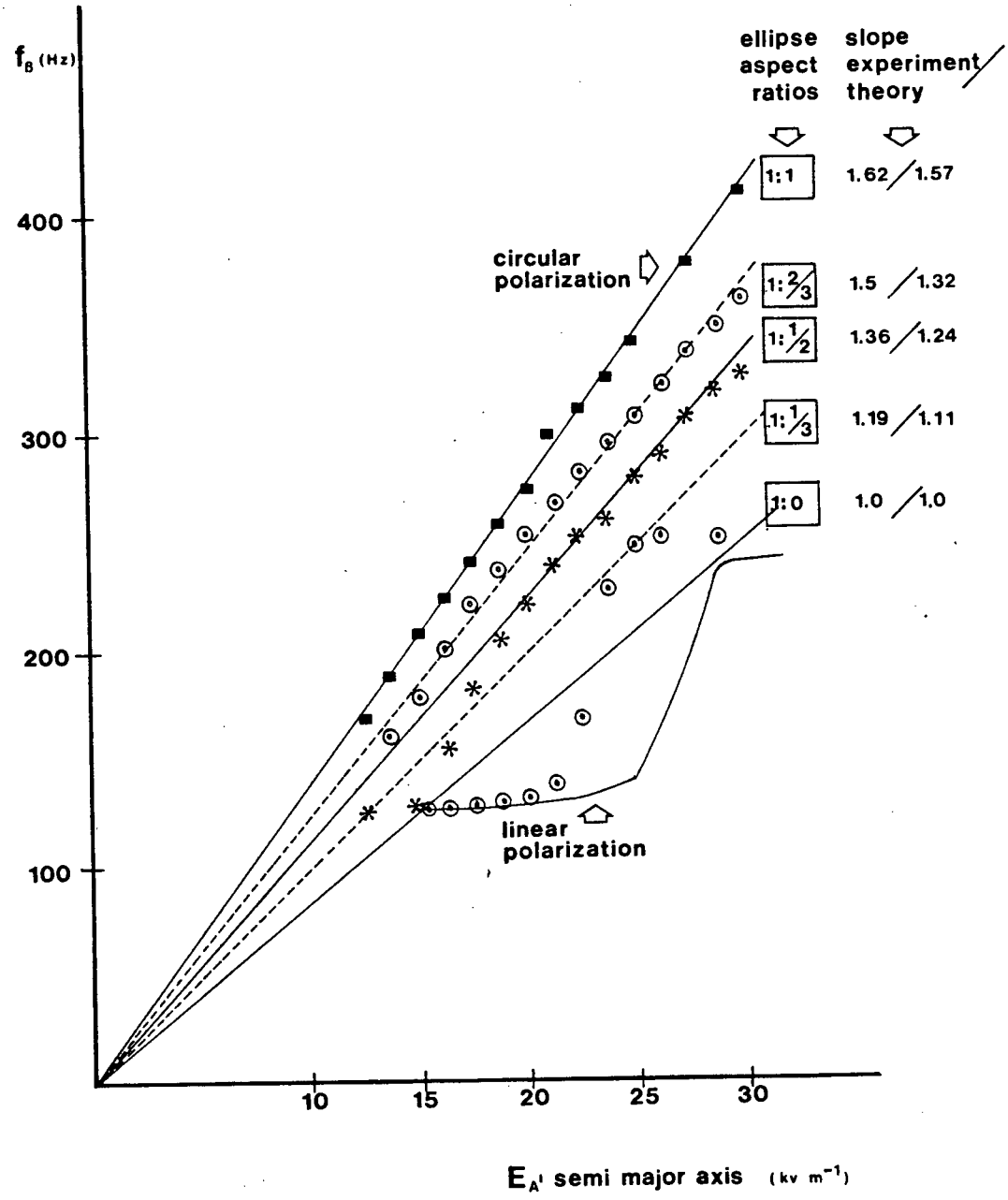

Figure 26 Pulse emission frequency as a function of applied field magnitude for different elliptically polarized fields. Slopes for lines are normalized to the slope of the line through the top of the steps of the calibration curve for the linear field. 38mm, 1.5 Torr Ar lead glass bulb.

5.5.2.3 Planar Rotating Fields and Penning Mixtures

This experiment is identical to the previous except the Penning bulb (Section 5.3.2) is used.

Linear field experiments (Section 5.3.2) revealed that a Penning bulb exhibits a very large pulse followed by progressively smaller and closer together pulses in each slope of the field. Extrapolating this to a continuously increasing field (ie. a ramp) which basically represents a circularly polarized field (ie. the change in E_A always has the same sign and occurs at a fixed rate) one expects a continuous glow (ie. no pulses). The continuous glow is maintained by a continuous replenishment of the metastable state. This result is exactly what is observed; no pulses just a weak D.C. light signal.

5.6 Investigations of Engineering Problems

Four basic types of experiments have been carried out: field perturbation due to the sensor, meter calibration stability, humidity effects and temperature effects*.

5.6.1 Field Perturbation

The purpose of this experiment is to find out how close to a conductor a bulb can be brought before the field is disturbed.

The experiment is performed with the 38mm diameter bulb filled to 0.66 Torr Ne. The applied field is a 60Hz sine wave of variable strength.

Calibration curves (f_B versus E_A) are obtained as a function of the distance, L, to one of the plates used in the capacitor. It is found that as the bulb is brought closer to the plate the count rate (f_B) increases for a constant applied field magnitude. Figure 27 shows the count rate as a function of distance from the plate. The maximum effect (touching the plate) is a 20% enhancement in the count rate. At distances greater than one bulb radius there is no effect.

Thus the sensor influences the measurement of the field up to a distance of one radius away from a planar conductor.

* the author did not participate in these temperature experiments.

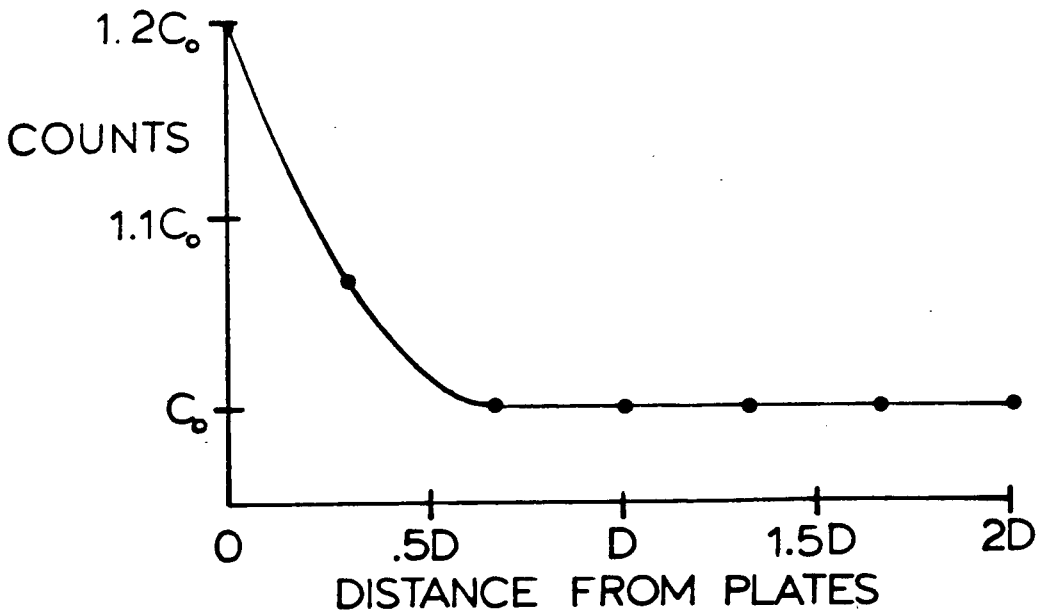

Figure 27 Response of Bulb Near one Plate of a Capacitor.

D = bulb diameter; C_o = counts at large distance from plate.

5.6.2 Meter Calibration Stability

A set of small plates identical to the large ones was constructed and placed outside the laboratory and shielded from the direct rain. The count rate for different bulbs at fixed field was monitored over the summer months.

A typical result is shown in Figure 28. The variation is less than 3%. Experiments such as these demonstrate that bulbs produce reliable results and remain calibrated for months.

5.6.3 Humidity Effects

This experiment is performed with a 25mm diameter pyrex bulb filled with .5 Torr of neon. The applied field is a 60Hz waveform whose amplitude can be varied. Relative humidities up to values of 95% can be obtained by directing the air from a humidifier on to the bulb. Higher relative humidities can be obtained by breathing on the bulb.

The operation of the sensor requires that the applied field penetrate the bulb material. As the humidity increases the glass conductivity increases and the applied field is screened from the gas. The effect can easily be observed by monitoring pulse emission while breathing on the bulb. A soon as the glass surface is fogged with the condensed water vapour, pulse emission stops altogether; as the water evaporates pulse emission returns to normal. Controlled experiments are hard to do in the laboratory due to water condensation on the plates. However two conclusion can be reached: (1) As the humidity increases the pulse rate decreases slowly at first and then rapidly for relative

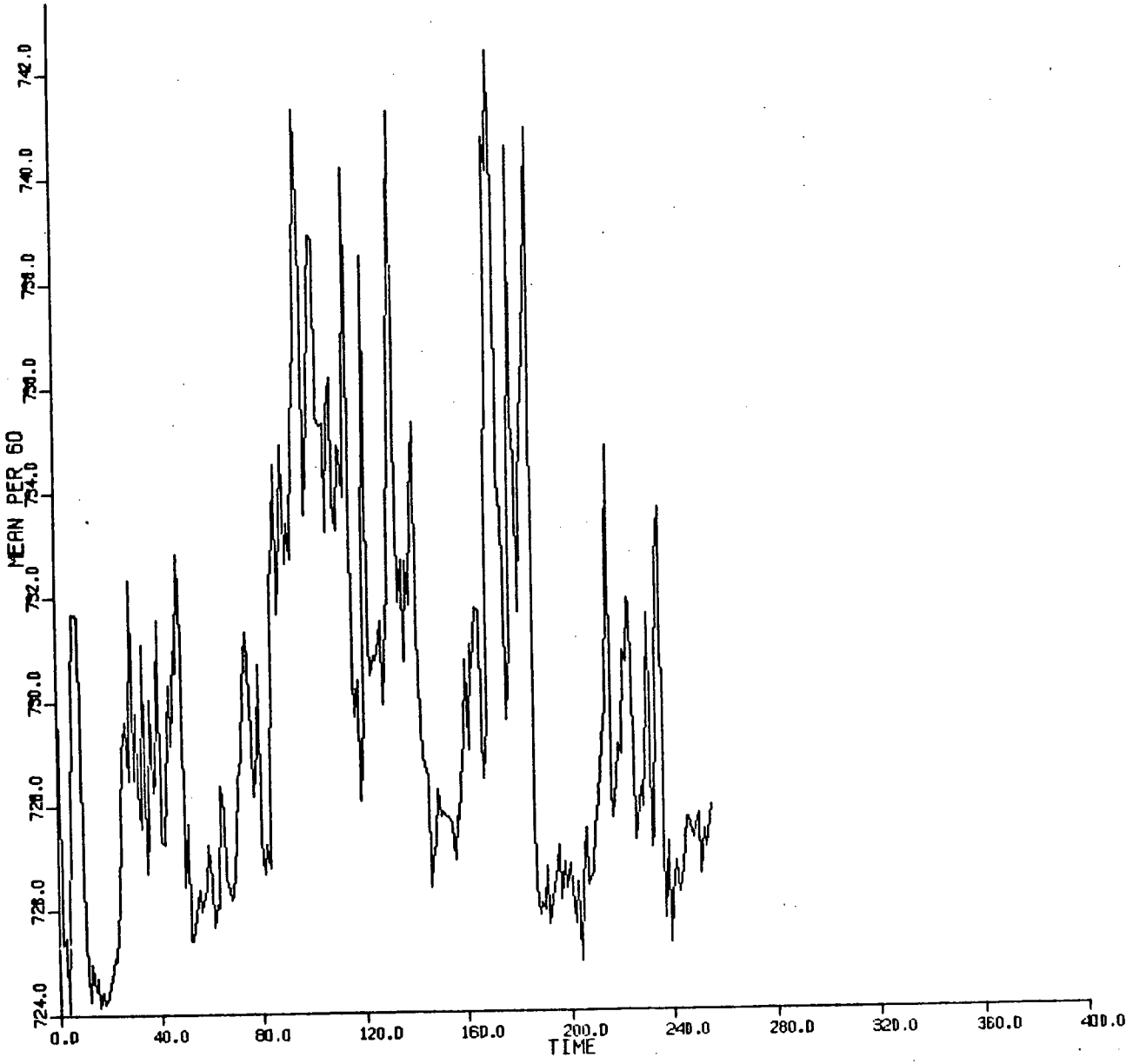

Figure 28 Overnight Run (June 7, 1982) showing counts versus time.

humidities above 95%; the effect is strongly dependent on how clean the bulb is. (2) Encasement of the bulb in a hydrophobic material such as teflon provides for reliable operation at relative humidities of at least 95% Breathing on the teflon holder has no effect. Field trials in light rain were also satisfactory.

5.6.4 Temperature Effects (Preliminary Results)

This experiment is performed by flowing dry air of varying temperature (-40°C to 40°C) around the bulb. The bulb is mounted in a plexiglass box to prevent condensation from occurring at low temperatures. From 0°C to 40°C no effect is observed. However from -40° to 0° dramatic changes are seen. Furthermore these changes are different for different bulbs. Results in this range are therefore still very inconclusive and further work is required.

5.7 Field Tests

The meter has been field tested at various times under transmission lines (265kV to 765kV), in substations and in high voltage laboratories. The purpose of these tests has been to confirm meter operation (mainly the detector) in noisy electrical environments.

Although initial prototypes revealed problems with detector shielding and optical fibre conductivity. the prototype described here has worked very well.

Because of the small field perturbation and size of the GEM sensor it has been possible to measure enhancement factors around the human body. The enhancement is about two when the sensor is placed in the shirt pocket and the person stands erect. When the sensor is placed on the head the enhancement ranges between 6 and 10 depending on the person and the exact position. These results are consistant with Deno's[8] theoretical calculations.

Other measurements have included the mapping of the electric field under transmission lines. Figure 29 shows a plot obtained by walking under a 500kV transmission line with a GEM fitted with a 100mm long cylindrical sensor. The general shape of the curve is as expected. Actual field magnitudes are hard to compare to theory because the height of the conductors varies greatly from place to place and the bulb reading is enhanced by the observer.

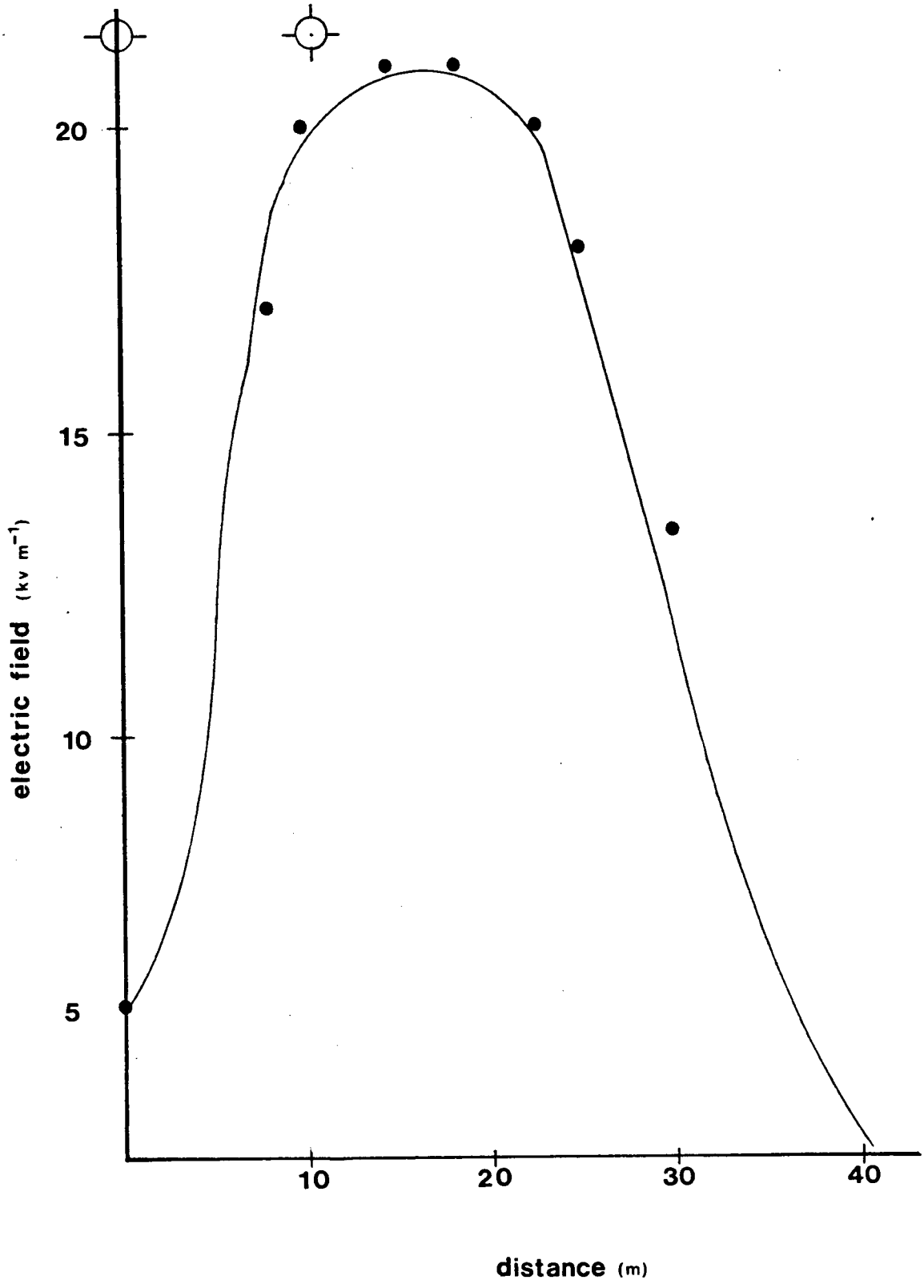

Figure 29 Electric Field Under a Typical 500kV Line Obtained With a 100mm Long Cylindrical Sensor About 2m Above the Ground.

5.8 Summary

This section has summarized experiments performed to develop GEM and the physical model for its sensor. Results show that the physical model makes predictions which are in good agreement with experimental results. However, some discrepancies are observed in planar rotating fields near threshold. These discrepanceis are likely due to the erroneous basic assumption of a uniform E_B. Results also shows the GEM meter operates reliably in typical environmental electric fields. However temperature effects observed below freezing are not understood.

6.0 Summary and Conclusions

Adverse health effects resulting from exposure to high electric fields in the vicinity of overhead transmission lines and switchyards are now a matter of considerable public concern. In addition direct accidents resulting from heavy equipment (ie. cranes) coming into contact with power lines are on the increase.

Existing electric field meters are not ideal for studying and monitoring environmental electric fields. The meters measure the induced charge or current between metal electrodes. As such the sensors are metallic, directionally sensitive and in most cases (where the electronics is housed with the electrodes) large and heavy.

This thesis describes an electric field meter based on a different principle: electrodeless breakdown of gases in insulating vessels.

This principle allows the construction of a meter with the sensor and detector separated by an optical fibre. The sensor consists of a glass shell filled with gas. As such the meter has the following advantages:

1. it is very light and small;
2. it is spatially isotropic or directionally sensitive (as desired);
3. it has no metal or conducting parts within an arbitrary distance from the sensor. The distance is set by the optical fibre length and
4. it remains calibrated for long periods of time (essentially because it uses a digital signal) and is not adversely affected by electrical noise.

Two types of sensors have been studied in detail: a spherical bulb and a cylindrical tube. The spherical bulb has a spatially isotropic sensitivity to the electric fields. For sufficiently small harmonic distortion, it responds only to the fundamental frequency component of the applied field. The response also depends on the polarization of the field. A cylindrical bulb responds to the component of the electric field along its axis irrespective of field polarization, and measures the greatest field strength along that direction. By suitably selecting the threshold field of the tube, one can discriminate entirely against field components which are normal to the tube-axis.

A meter fitted with a cylindrical tube is most suitable for accurately measuring components of the electric field and thus fully characterizing the field. A meter fitted with a spherical bulb, on the other hand, is best suited for less accurate applications in which careful orientation of the sensor is not possible. The measurement provided by the spherical bulb is dependent both on the magnitude and the geometry of the field. Thus it does not uniquely characterize the field.

For either type of sensor there is a threshold below which the electric field cannot be detected. The threshold depends on the type of gas and the bulb dimension. For a given type of gas a larger bulb has a lower threshold. This property, although very advantageous for threshold control, is the main limitation on the meter. A reasonable size sensor (40mm bulb diameter) has a threshold of about 10kV/m. This field is slightly higher than typical unperturbed fields found at ground level near power lines and switchyards. Thus to measure these low fields a larger sensor is required. On the other hand very small bulbs (a few millimeters) can be made and even though they have a very large threshold they can be used in unique situations as discussed later on.

Although the basic theory of electrodeless breakdown was developed by Harries and von Engel based on Townsend's work this thesis extends their work both into more basic physics and engineering aspects.

The study of electrodeless breakdown had been confined to the basic explanation of why current pulses occur when the gas is exposed to an electric field. This thesis extends the basic physics to a theoretical explanation of:

1. the relation between the frequency of light pulses (f_B) and the applied field (E_A);
2. the effect of gas pressure on f_B versus E_A;
3. the dependence of f_B on E_A in elliptically polarized fields ranging from linear to circular polarization;
4. the effects of the geometry and orientation of bulbs on the dependence of f_B on E_A;
5. the effects of harmonics on f_B versus E_A and
6. the breakdown effect in Penning mixtures.

This thesis also presents many new engineering results:

1. environmental effects on the performance of the sensor and meter;
2. lifetime and stability of the meter;
3. meter design to reduce electrical noise and protect the sensor against environmental effects and handling and
4. the influence of the sensor on the field being measured.

Even with all these extensions much work remains to be done both on the study of the phenomena and on meter design.

There are at least three areas of the basic phenomena that require further study: bulb construction, temperature effects and operation in

planar rotating fields. The first two areas are most likely related and by far the most important from a practical point of view. Although similar bulbs can be made routinely with a yield rate of about 70% no two bulbs are alike. They have slightly different thresholds and calibration curves. This is a problem in the commercial exploitation of the meter, because each bulb must be calibrated and each detector adjusted to the bulb (ie. the mean pulse height is different for different bulbs). Temperature effects below freezing are also not yet understood. It is presently believed that they are due to the adsorption of impurities at low temperatures. If this is the case reproducible bulbs with no temperature effects could be produced by proper control of impurities during manufacture. Finally, a rigorous quantitative model for the operation of spherical bulbs in plannar rotating fields could be developed. The main problem here is understanding the form of the non uniform internal bulb field E_B. However, this more rigorous model may have little practical application. With present understanding it is clear that spherical bulbs will need to be calibrated for each field geometry.

Future work on meter design will be guided by market developments. The present prototype which consists of a typical size sensor (40mm) separated by an optical fibre from the detector is well suited for demonstrations and field tests. However, the design must be modified for specific applications. The main parameters that can be changed are: the sensor dimensions (keeping in mind the effect on threshold) and geometry, the fibre length (including zero length or no fibre) and the detector size (if miniaturization is desired) and type. Making these changes may be harder than apparent. For example a very small sensor or a long fibre

may required larger gain in the detector. Table 3 summarizes possible applications for different fibre lengths and detector types (ie. different electronics for conveying the electric field information). The major applications are for monitoring and warning devices. As mentioned before one of the major limitations is threshold. However in most applications in which low fields need to be measured (ie. personal warning or monitoring) the unperturbed (low) field is enhanced greatly by the presence of conducting objects and therefore usually detectable. Other totally different applications have recently appeared. These applications encompass areas of electric field measurement which cannot be done at all with existing devices. These applications require a very small (few millimeters) non metallic sensor (ie. in other applications metal is dangerous but can be used). One example is measurement of electric fields inside beehives (the first device sold was for this application). Another more promising application is the measurementof fields inside (in oil) large transformers. These measurements may assist in predicting possible future transformer malfunctions during transformer assembly.

Table 3

Meter Configurations and Applications

fibre length / detector	no fibre (one package)	short fibre (< 2 meters)	long fibre (> 2 meters)
warning device	Personal warning device (workmen)	Testing vicinity of live high tension line (crane operators, hydro repair-men, etc.)	
direct read out	Hand held field measurement device (workmen, researchers, evaluators)		Unperturbed accurate field measurement Line testing (workmen, researchers)
micro-processor	Unsupervised field monitorying (operators, researchers) Personal exposure meter (workmen)	Personal exposure meter (workmen)	Unperturbed field meeasurements over long periods of time (researchers, eval-uators)
histogram device	same as microprocessor but only compiles a histogram (ie. no time resolution)		

7.0 References

1. Kronberg H.A., Concern Overhead, EPRI j., Vol. 5, No. 7, pp 7 - 13, June/July, 1977

2. New York State Public Service Commission Cases 26529 and 26559 conducted over the period 1975 to 1978, New York State Public Service Commission (Albany, N.Y.)

3. Banks, R.S., Kanniainen, C.M., and Clark, R.D., Public Health and Safety Effects of High-Voltage Overhead Transmission Lines: An Analysis for the Minesota Environmental Quality Board, Minesota Department of Health, October 1977

4. Presman, A.S., Electromagnetic Fields Life (translated from Russian) 1970, Plenum Press, New York

5. Janischewskyj, W. and Stopps, J.G., "An Epidemiological Study of Personnel Working on ac Transmission Lines", Conference of the CEA, Vancouver, B.C., March, 1979

6. Kotler, R.F., Misokian, M., AC Transmission Lines Field Measurements, Institute for Basic Standards, NBS, Washington, D.C., November, 1977

7. "Evaluation of Proximity Warning Devices, South-West Research Institute, February 22, 1980

8. Deno, W.D., Currents Induced in the Human Body by High Voltage Transmission Lines Electric Field - Measurement and Calculation of Distribution and Dose, IEEE Transactions on Power Apparatus and Systems, Vol. PAS-96, N.J. September/ October, 1977

9. Speigel, R.J., Kerns, D.R., Cooper, E.H. and Bronaugh, E.L., "A Small, Accurate, Optically Isolated Electric Field Probe", IEEE PES Summer meeting, Vancouver, B.C., July 15-20, 1979

10. Francis, G., "Ionization Phenomena in Gas", Butterworth Publications (London) 1960, pp. 137-172

11. Harries, W.L. and von Engel, A., Proc. Phys. Soc. B64, 915 (1951)

12. Harries, W.L., Proc. I.E.E.E. IIA, 100, 132 - 7 (1953)

13. Harries, W.L. and von Engel, A., Proc. Roy. Soc. (London) A-222, 490 (1954)

14. Dutton, J., in Electrical Breakdown in Gases, edited by J.M. Meek and J.D. Craggs (Wiley, New York, 1978), pp. 209-318

15. Friedmann, D., Curzon, F.L. and Young, J.F., A New Electrical Breakdown Phenomenom in gas-filled Insulating Bulbs, Appl. Phys. Lett 38(6), 15 March 1981. (Erratum App. Phys. Lett. 39(8), 15 October 1981)

16. Curzon, F.L., Friedmann, D.E., Feeley, M. Orientation - Dependent Electrodeless Breakdown of Gas in Glass Tubes, Journal of Applied Physics (In PressDecember 1982)

17. Friedmann, D.E., Curzon, F.L., Feeley, M., Young, J.F., and Auchinleck, G., An Electric Field Meter Based on the Breakdown of Gases, Rev. Sci. Instr. 53, 1273 - 1277, 1982

18. Friedmann, D.E., Curzon, F.L., and Feeley, M. Electrodeless Breadown of Gas in Rotating Electric Fields at 60Hz, in preparation for submission to the Canadian Journal of Physics

19. Young, J. and Friedmann, D.E., Electric Field Detector, U.S. Patent Application No. 06/142, 815, filed 22 April 1980

20. Holloway, D.G., "The Physical Properties of Glass", Wykeham Publications (London) Ltd., 1973, Chapter 3.

21. Lorrain, P., and Corson, P., "Electromagnetic Fields and Waves", San Francisco, W.H. Freeman and Co., Chapter 4, Figure 4.22, pg. 169, 1970

22. Da Silva, L., "A Rotating Electric Field Device", 4th year engineering physics project, UBC, January 4, 1982

23. Jackson, J.D., "Classical Electrodynamics", New York, John Wiley and Sons, 1975, Chapter 2, pp. 60 - 62

APPENDIX I

Effects of Finite Conductivity

For the purposes of this Appendix it is assumed that the spherical shell consists of glass in which surface conduction of leached ions in absorbed water is the main charge transport mechanism[20]. This means that the ions move as a result of the electric field (E_θ) tangential to the surface of the sphere. It is also assumed that ohmic conduction occurs (ie. $v = \beta E_\theta$, where v is the ion velocity, and, β, the mobility), and that there is no net charge on the sphere. Positions on the sphere are described by right hand spherical polar co-ordinates a, θ and ϕ. A spatially uniform oscillating field, $E_A' e^{j\omega t}$ is applied along the z-axis of the shell, as shown in Figure I, where ω is the frequency, t the time and $j^2 = -1$. The poloidal field E_θ is therefore given by the expression.

$$E_\theta = -E_A' e^{j\omega t} \sin\theta - (1/a)(\partial V/\partial\theta) \qquad \text{(I-1)}$$

where the potential V at point P (Figure I) results from motion of charges over the surface of the shell. These charges have a density of σ coulombs m^{-2} so that V satisfies the equation,

$$V = \int \sigma \, d\Sigma / 4\pi\varepsilon_o R \qquad \text{(I-2)}$$

where $d\Sigma$ is an element of area at Q (Figure I), R is the distance from Q to P, and ε_o is the permittivity of free space. The domain of integration is

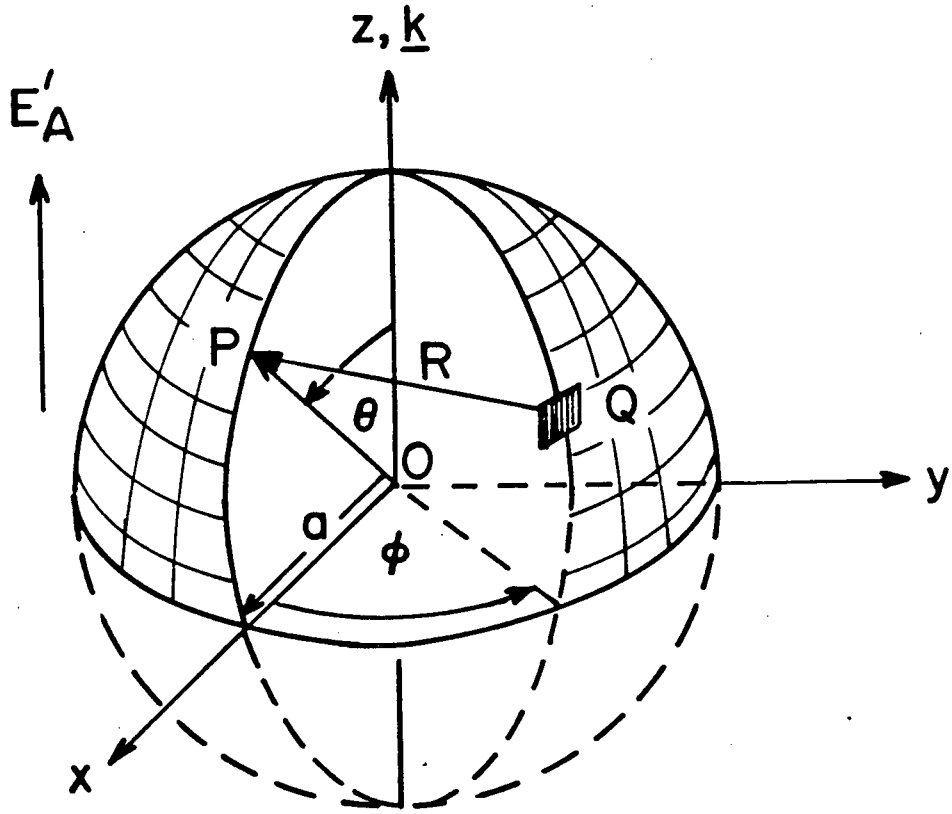

Figure I Geometry of the conducting shell in the applied field (E_A').

surface of the shell. Change conservation requires that σ satisfy the following equation:

$$a\Omega \sin\theta(\partial\sigma/\partial t) + \partial(E_\theta \sin\theta)/\partial\theta = 0 \qquad \text{(I-3)}$$

where Ω is the resistance of the shell in ohms per square. Using this equation to eliminate σ from (I-2) enables V to be expressed in terms of E_θ as follows:

$$\partial V/\partial t = -\int (4\pi\varepsilon_o aR\Omega \sin\theta)^{-1} (\partial E_\theta \sin\theta/\partial\theta) d\xi \qquad \text{(I-4)}$$

By differentiating (I-1) with respect to time $\partial V/\partial t$ can be eliminated from (I-1) and (I-4) to yield an integral equation for E_θ, namely;

$$\partial E_\theta/\partial t = -j\omega E_A' e^{j\omega t} \sin\theta + (\partial/\partial\theta)\int K\, d\xi \qquad \text{(I-5)}$$

where

$$K = (4\pi a^2 \varepsilon_o R\Omega \sin\theta)^{-1} (\partial E_\theta \sin\theta/\partial\theta) \qquad \text{(I-6)}$$

To solve the equation we write

$$E_\theta = \alpha E_A' (\sin\theta) e^{j\omega t} \qquad \text{(I-7)}$$

where α is a constant which is to be determined. With this assumption equation (I-5) becomes

$$\alpha \sin\theta = -\sin\theta + \partial/\partial\theta \int (2\pi j\omega a^2 \varepsilon_o R\Omega)^{-1} \alpha(\cos\theta) d\xi \qquad \text{(I-8)}$$

The integral can be evaluated by noting that it is related to the poloidal field E'_θ produced by a surface charge density σ' of the form $\sigma' = c \cos\theta$. From Jackson's solution[23] to the problem regarding the effect of a constant field applied to a conducting sphere, it is readily shown that

$$E'_\theta = -(\partial/\partial\theta) \int c(\cos\theta)\, d\xi/4\pi\varepsilon_o\, aR = (c \sin\theta/3\varepsilon_o) \qquad \text{(I-9)}$$

Comparing the integrands in (I-8) and (I-9) it is apparent that equation (I-8) can be written as

$$\alpha \sin\theta = -\sin\theta - 2\alpha \sin\theta/3j\omega a\varepsilon_o\Omega \qquad \text{(I-10)}$$

Hence

$$\alpha = -1[1 - j(\omega'/\omega)]^{-1} \qquad \text{(I-11)}$$

where

$$\omega' = 2/(3a\varepsilon_o\Omega) \qquad \text{(I-12)}$$

Using (I-17), (I-11) and (I-3) shows that the surface charge density σ is given by the equation,

$$\sigma = 2E'_A(\cos\theta)\, e^{j\omega t}/[a\Omega(j\omega+\omega')] \qquad \text{(I-13)}$$

Again having recourse to Jackson's book it is readily shown that this surface charge produces a uniform field $\underline{E_C}$ in its interior given by the equations:

$$\underline{E}_C = -w' E'_A \underline{k} e^{jwt}/(jw+w') \qquad \text{(I-14)}$$

where $\underline{k}$ is a unit vector along the z-axis (Figure I-1).

Hence the total applied field inside the shell (E_T) is

$$\underline{E}_T = \underline{E}_C + \underline{E}_A = jwE'_A e^{jwt}\, \underline{k}/(w' + jw) \qquad \text{(I-15)}$$

For a field of strength E'_A, switched on at time t = 0 it is readily shown that for $t > 0$

$$E_T = E'_A e^{-w't} \qquad \text{(I-16)}$$

Equation (I-15) shows that $\underline{E}_A$ is attenuated by the conducting shell ($E_T = E'_A\,[1 + (w'/w)^2]^{-1/2}$) and is also phase shifted by an angle ϕ where $\tan \phi = (w'/w)$. For the case of interest ($w' \ll w$), only the phase shift is significant.

APPENDIX II

Rate of Pulse Emission in Planar Rotating Fields

In a linearly polarized field (an elliptical field with unit eccentricity) the bulb obeys relation (2). In elliptical or circularly polarized field however it is necessary to extend the basic theory. Assuming the basic phenomena remains the same and that the internal field (E_B) in the bulb caused by charge separation is uniform, then a new breakdown still occurs every time the applied field changes by E_o, however the addition of the fields is now vectorial. For breakdown one must have

$$|\underline{E}_A + \underline{E}_B| = E_o \qquad \text{(II-2)}$$

To proceed further it is assumed that the phasors for E_A (and E_B) are elliptical with major axis

$$E_A = \gamma E_o, \qquad \text{(II-3)}$$

and minor axis,

$$\beta E_A = \beta \gamma E_o \qquad \text{(II-4)}$$

where γ is a factor which determines the ratio of the applied field amplitude E_A, to the breakdown voltage of the gas. For $\gamma < 1$, breakdown does not occur. With these variables the fields can be described parametrically by the angles, A and B and the equations

$$\underline{E_A} = \gamma E_o((\beta \sin A)\,\underline{i} + (\cos A)\underline{j})$$
$$\underline{E_B} = -\gamma E_o((\beta \sin B)\underline{i} + (\cos B)\underline{j} \qquad \text{(II-5)}$$

where $\underline{i}$ is a unit vector along the minor axis of the phasor and $\underline{j}$ is a unit vector along the corresponding major axis. It follows from equations (II -5) that the magnitude of $\underline{E_A} + \underline{E_B}$ is given by the expression

$$|\underline{E_A} + \underline{E_B}|^2 = \gamma^2 E_o^2\,(\beta^2(\sin A - \sin B)^2 + (\cos A - \cos B)^2)$$

Since $|\underline{E_A} + \underline{E_B}| = E_o$ at breakdown it follows from the above result that, at breakdown, B satisfies the equation

$$(1/2\gamma) = \sin((A-B)/2)[(1-\beta^2)\sin((A+B)/2)+\beta^2]^{1/2} \qquad \text{(II-6)}$$

For $\beta = 0$ (linearly polarized fields) the above equation reduces to the form

$$1=\gamma(\cos B - \cos A), \text{ or } E_A(\cos B - \cos A) = E_o \qquad \text{(II-7)}$$

Since $E_A \cos B$ and $E_A \cos A$ are the components of the fields along the major axis of the ellipse, equation (II-7) is consistent with equation (II-1). For $\beta = 1$ (circular polarization) equation (II-6) also has the simple solution

$$(1/2\gamma) = \sin((A-B)/2) \qquad \text{(II-8)}$$

The angle through which E_A rotates between successive breakdowns is however, A-B. It therefore follows that the number of breakdowns per cycle, f_B, is $2\pi f_A/(A-B)$ or,

$$f_B = \pi f_A / \sin^{-1}(1/2\gamma) \qquad \text{(II-9)}$$

Comparing this result with equation (II-1) shows that, for strong fields ($\gamma \gg 1$) the breakdowns per cycle is increased in going from linear to circular polarization for fields of constant amplitude. In fact, as $\gamma \to \infty$

$$f_C/f_L \to \pi/2 \qquad \text{(II-10)}$$

where f_C and f_L and the respective number of breakdowns per second in circularly and linearly polarized fields at the same field strengths. For more general cases of elliptical polarization, equation (II-6) can be reduced to a quartic equation for B, and has either 0, 2 or 4 real solutions. For successive breakdowns B is the smallest real solution which exceeds A. In the limiting case of very strong fields E_o becomes an element of arc length of the phasor. Hence the enhancement ratio resulting from the elliptical field becomes

$$f_E/f_L = E(m_1) \qquad \text{(II-11)}$$

where f_E is the frequency of breakdown in the elliptically polarized field and $E(m_1)$ is an elliptic integral of the second kind, with $m_1 = 1-\beta^2$. This result is analogous to that obtained for a circularly polarized field. For an ellipse $E(m_1)$ is the length of a quadrant of the elliptical phasor. For the circular polarization $m_1 = 1$ and $E(1) = \pi/2$ as expected. To gain more insight concerning the effects of changing the polarization of the field equation (II-6) has been solved iteratively with a computer. The calculation is begun by selecting β, γ and an initial value of B (B_1 say). A solution is

obtained for A (A_1), and B is then reset to the value A_1. The process is repeated for twenty successive breakdowns. The angle $\phi(n)$ between the bulb field (E_B) and the $\underline{j}$-axis (Figure 6) is then evaluated on the nth iteration using the result

$$\phi(n) = \arctan(\beta \tan B_n) \qquad \text{(II-12)}$$

The average angle $\bar{\phi}$ through which $\underline{E}_A$ rotates for breakdown is then given by

$$\bar{\phi} = (\phi(20)-A_1)/20 \qquad \text{(II-13)}$$

and the standard deviation, ϵ, by the expression

$$\epsilon^2 = \sum_{j=1}^{20} (\phi(n)-\bar{\phi})^2/20. \qquad \text{(II-14)}$$

(The standard deviation gives information on the variability in the time interval between breakdowns). The number of breakdowns per second is thus

$$f_B = 2\pi f_A/\bar{\phi} \qquad \text{(II-15)}$$

Figure II shows graphs of f_B for β = 1, .66, .5, 0.33 and 0.

The significant features of the response curves are as follows:

1. as β increases from 0 (linear polarization) to 1 (circular polarization) the graphs become progressively less "stepped" in form;
2. the graphs become smoother at successively larger values of γ as β is decreased;

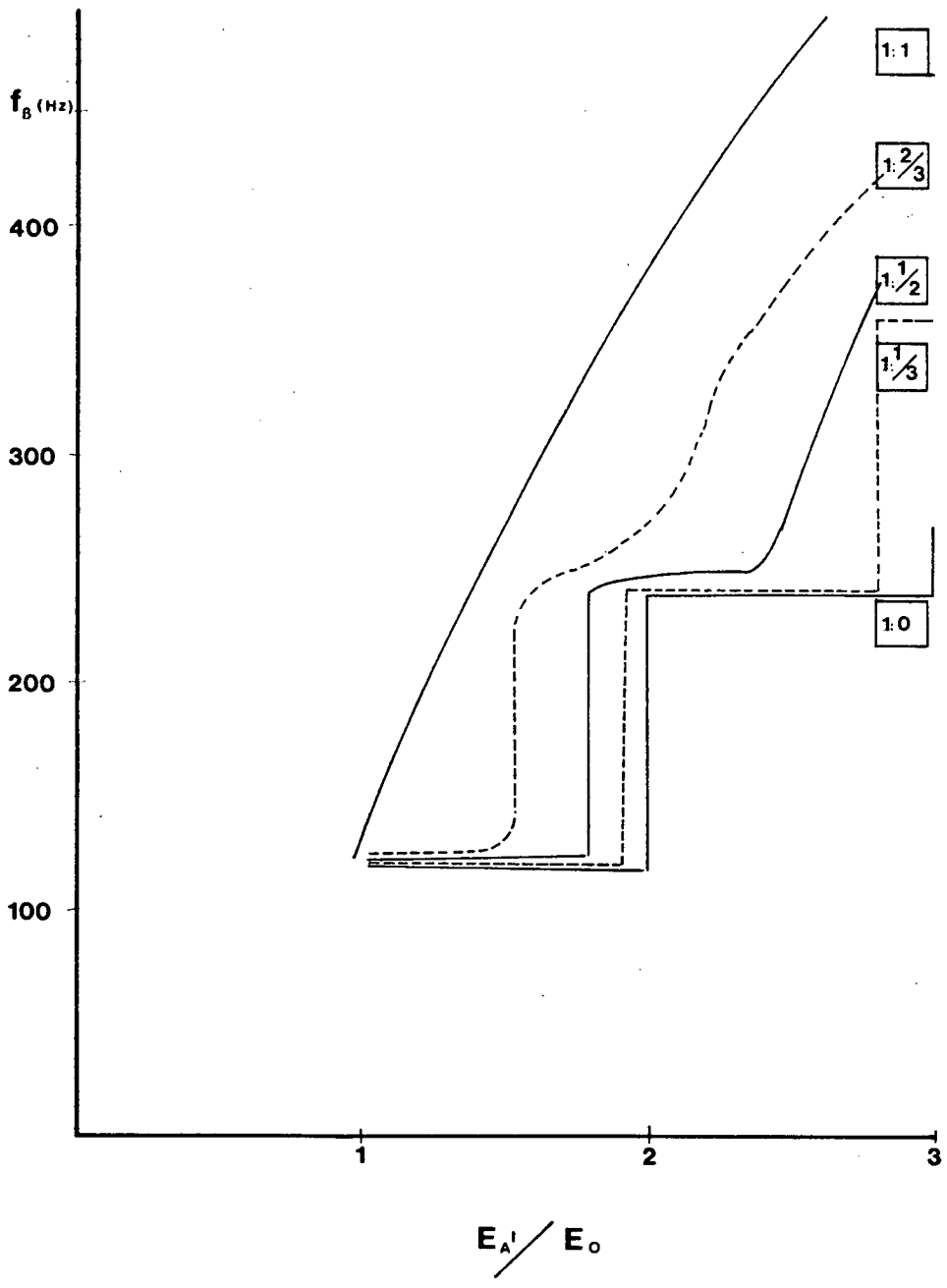

Figure II Pulse Emission as a Function of Normalized Applied Field Magnitude for Different Elliptically Polarized Fields. Theoretical Result Assuming E_B is uniform. Compare with Figure 26.

3. the curves all start at the same point (ie. the threshold field strength, and breakdown frequency at threshold are independent of polarization);
4. at high field strengths, the response curves are asymptotic to straight lines which pass through the origins. The model also shows that the breakdown frequency at large fields is enhanced by a factor f_E/f_L, in comparison to the value of f_B observed with linearly polarized fields. The largest enhancement is $\pi/2$ and occurs in the case of circular polarization.